Australian Government

ANSTO

Multi-wavelength Absorption Black Carbon Instrument (MABI) Manual

Armand J. Atanacio, David D. Cohen, Madhura Manohar
David Button, Nikolas Paneras, David Garton

Australian Nuclear Science and Technology Organisation

CONTACT DETAILS

ANSTO	Australian Nuclear Science and Technology Organisation
Postal Address	Locked Bag 2001, Kirrawee DC NSW 2232, Australia
Telephone	+61 2 9717 3111
Website	www.ansto.gov.au

CONTENTS

Main Components Overview

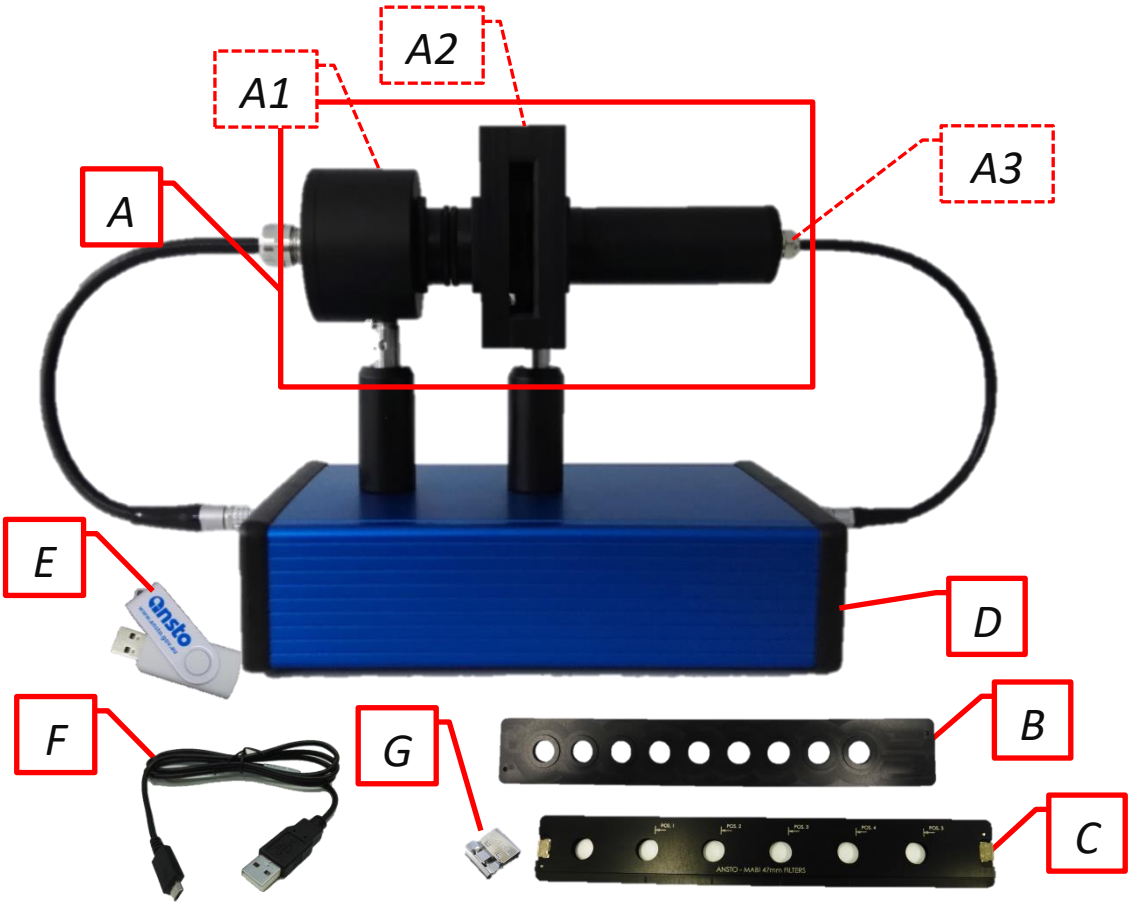

Figure 1. Image of the main MABI harware components.

A	Optical assembly
A1	Seven-wavelength light assembly: 405nm, 465nm, 525nm, 639nm, 870nm, 940nm and 1050nm (referred to as "light source")
A2	Sample holder slot
A3	Photo detector
B	25mm diameter filter holders with 9 filter positions
C	47mm diameter filter holders with 6 filter positions
D	Instrument electronics case
E	MABI USB Stick/Drive with required software to run
F	Micro-USB to USB cable to connect D to your computer USB port.
G	Push-pull quick release filter holder clips used on sticks B and C

Important Information

Safety Warning

It is highly recommended to power off the instrument before performing any maintenance. The LED light source can produce fluxes above 1mW that has a potential to damage eye sight.

Minimum Computing Requirements

Operating System

- This instrument is designed to run on computer using Windows 7 and above
- USB 2.0 or higher

Environmental Conditions

It is recommended to store and operate the instrument in Laboratory type conditions. Ideal conditions include temperatures of (22 ± 5)°C degrees and a relative humidity of (50 ± 10) %. The instrument also has sensitivity to external light sources. It is import to operate in lower light levels that are white and non-changing.

Full MABI Package Contents

1x Instrument storage case
1x MABI hardware assembly
2x 47mm diameter filter holder
2x 25mm diameter filter holder
1x MABI USB drive (contains software application and manuals)
1x micro-USB to USB cable
10x Filter holder clips

NOTE: A desktop computer or laptop computer is required to operate the MABI instrument. This computer is NOT provided as part of the MABI package and must be supplied by the user.

Introduction

The awareness of fine particle matter (PM) air pollution on a local, regional and global scale has increased significantly over the past decade around the world. It is now widely accepted that the air we breathe every day is polluted to various degrees by particulate matter (PM) released into the atmosphere by motor vehicles, factories, power stations and even home wood fire heaters. These fine aerosols, less than 2.5µm diameter (PM2.5), are known to contribute to reduced visibility, degrade outdoor cultural heritage monuments and even affect global climate change through the absorption and reflection of solar and terrestrial radiation. A growing body of scientific literature continues to identify strong links between fine particulate matter (PM2.5) and a wide range of adverse human health conditions and even premature death. In fact, in October 2013 the World Health Organisation's - International Agency for Research on Cancer (IARC) formally classified "Particulate Matter, a major component of outdoor air pollution, as carcinogenic to humans (Group 1)". Consequently, the monitoring of fine particle pollution concentrations and their related sources has become increasingly important for governments and regulatory bodies around the world.

One of the most significant constituents of atmospheric fine particles is black carbon (BC), sometimes referred to as elemental carbon (EC), light absorbing carbon (LAC) or soot. It typically represents 10-40% of the PM2.5 mass fraction based on studies in Australian urban areas (Cohen et al. 1995, 1995b, 1996, 1999, Ayers et al. 1998). One could therefore reasonably expect this fraction to be significantly higher in highly urbanised regions such as Asia. According to Horvath (1993, 1997b), it is also responsible for up to 90% of the light absorption in the atmosphere. Black carbon is clearly a very important aerosol component to measure correctly.

A widely accepted technique for measuring the BC component of an exposed filter sample is known as the Laser (633nm) Integrated Plate Method (LIPM), the details of which can be found in Cohen et al. 2000 (provided in the appendix). It is important to note that the Laser absorption method relies on a mass absorption coefficient which is a strong function of the particle size, refractive and density of the BC particles, as well as the wavelength of light used. As fine BC can be generated from a range of different sources, its particle size and density distribution may also vary in a collected sample depending on the dominant sources of BC at the site.

The Multi-wavelength Absorption Black Carbon Instrument (MABI) automatically performs this absorption technique at the following seven (7) wavelengths: 405nm, 465nm, 525nm, 639nm, 870nm, 940nm and 1050nm. Using the absorption data from different wavelengths, it is possible to differentiate the different BC size fractions originating from sources such as wood smoke or motor vehicles.

MABI Assembly Instructions

Optical Components

The main hardware components of the MABI, including optical system and electronics, come preassembled and only require connection of the data communication cables. The individual hardware components should not be disassembled under normal instrument use in order to retain the correct optical alignment and calibration.

The individual optical assembly consists of the multi-wavelength light source (containing 7 default wavelengths: 405nm, 465nm, 525nm, 639nm, 870nm, 940nm and 1050nm), sample holder slot and photo-detector.

Perform the following steps to connect the data communication cables:

(1) Locate the male plug at the end of the cable attached to the multi-wavelength light assembly (**Figure 1** - **A1**) and attach it to the female plug on the MABI electronics case (**Figure 1** - **D**). Note; ensure the red dot markers are aligned to ensure the correct orientation of the plug before inserting it to avoid damaging the cable pins, see **Figure 2** below.

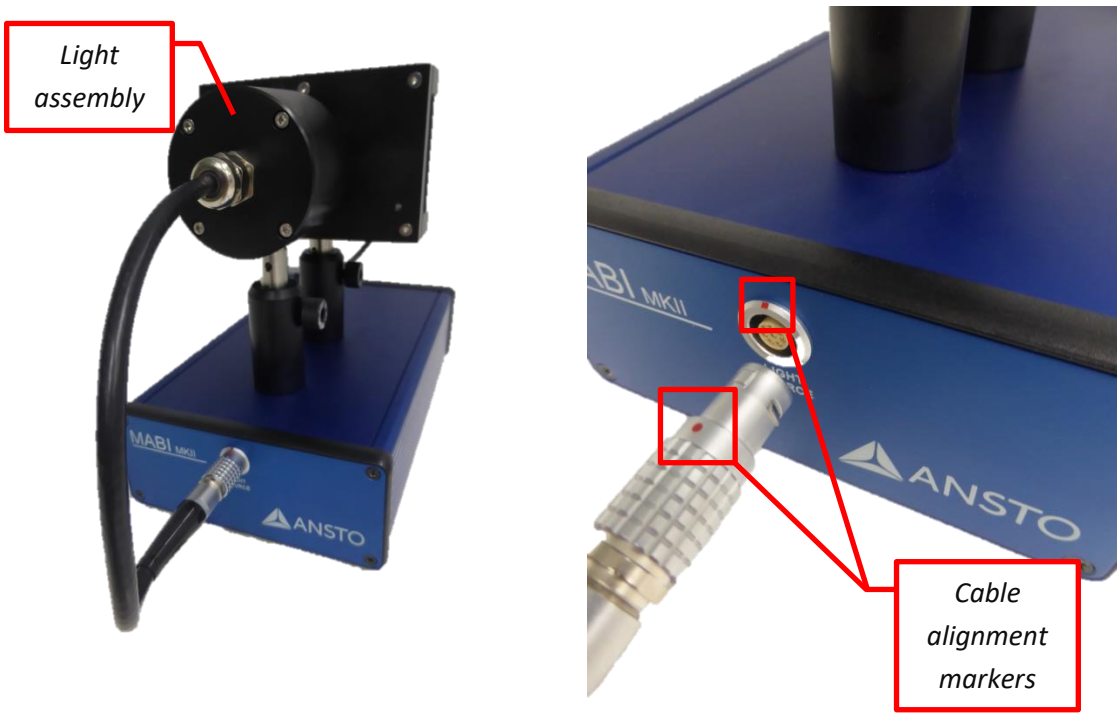

Figure 2. Images of the light assembly cable installation.

(2) Locate the male plug attached to the photo-detector (**Figure 1** - **A3**) on the opposite end of the MABI and attach it to the female plug on the MABI electronics case (**Figure 1** - **D**). Note; ensure the red dot markers are aligned to ensure the correct

orientation of the plug before inserting it to avoid damaging the cable pins, see **Figure 3** below.

.

Figure 3. Images of the photo-detector and USB cable installation.

(3) Locate the USB cable provided and attach the micro-USB end to the port on the electronics case (**Figure 1 - D**). Attach the full-sized USB end of the cable to an empty USB port on your computer. This cable provides data transfer from the MABI to the computer as well as power to the MABI instrument.

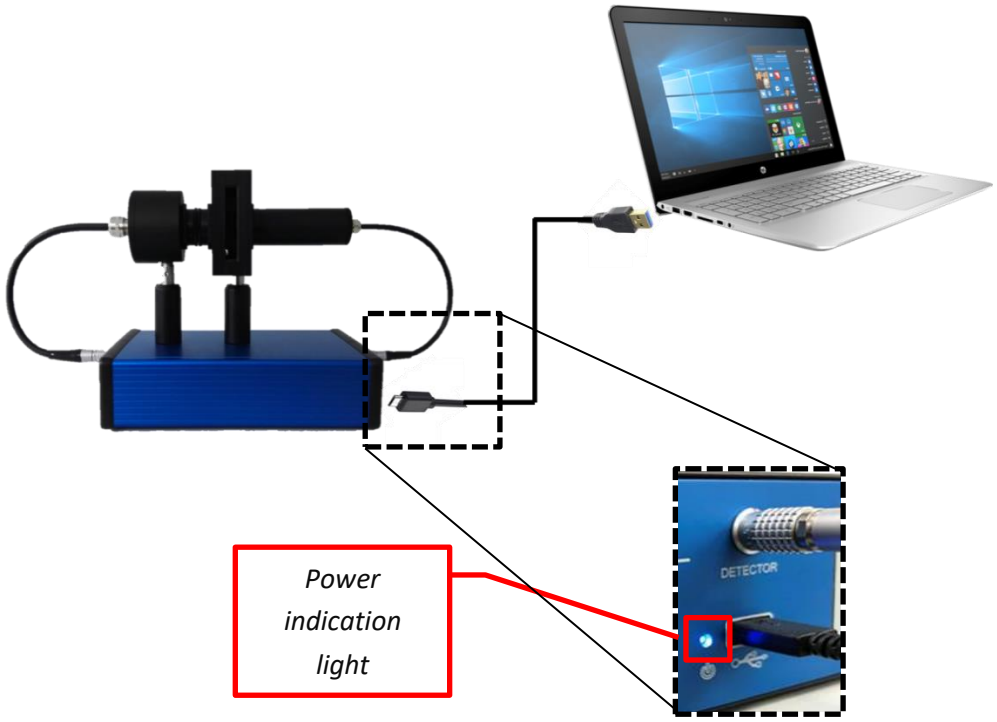

Figure 4. Schematic diagram of the MABI unit hardware cable connections.

Power-up System Hardware

There is no power on/off switch on the MABI unit. The MABI system will automatically power-up as soon as the USB from the MABI is attached to a functioning computer. This is indicated by illumination of the blue LED on the electronics case, see Figure 4 above.

Congratulations. The hardware has now been successfully assembled.

Software Application Installation

Now that the hardware is assembled, the following steps will take you through installation of the MABI software application.

Steps:

(1) Insert the MABI USB Stick/Drive (**Figure 1** - **E**) and (**Figure 5**) into your computer.

Figure 5. ANSTO USB drive containing MABI software and associated files.

Open the **MABI DAQ V2.20** folder.
*(**Note:** you will require administrator rights on your computer to install the software)*

Locate and execute **Setup.exe**

This will launch the software installer as shown in **Figure 6**. Please do not click or select other function just wait until the progress bar reaches 100% and follow any subsequent instructions and progress screens to complete the installation as shown below in **Figure 6** to **Figure 13**.

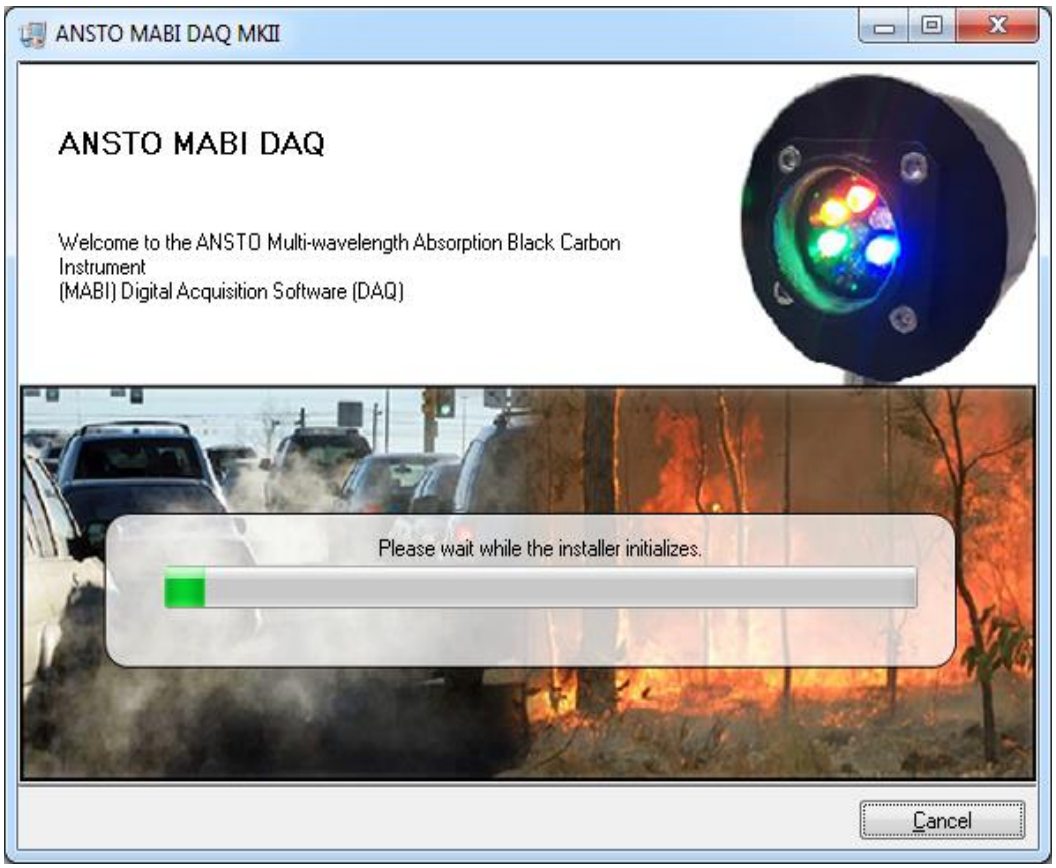

Figure 6. Image of the MABI software installation screen.

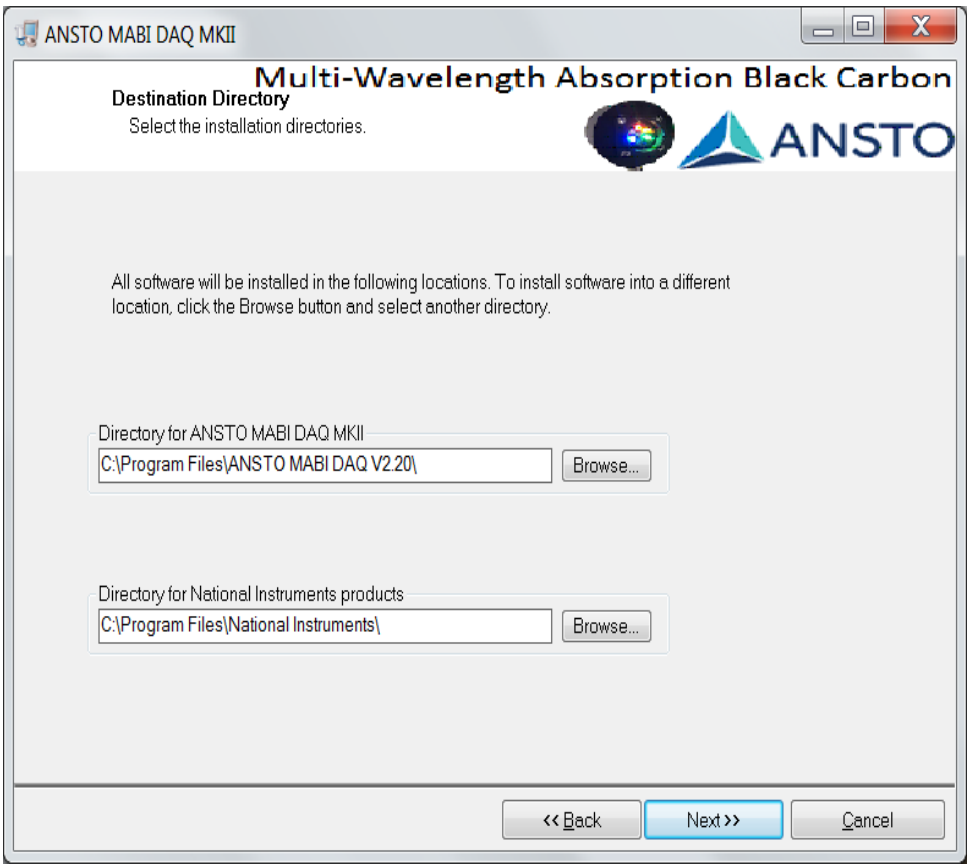

Figure 7. Image of the destination directory screen.

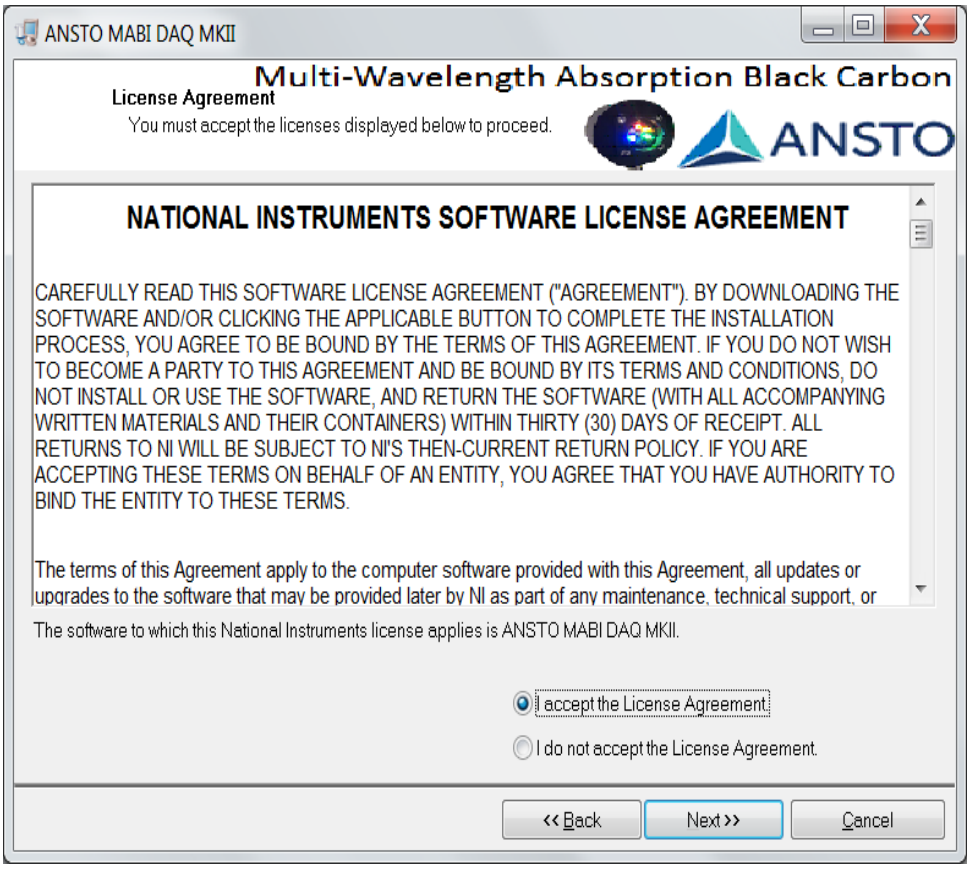

Figure 8. Image of the licence agreement screen.

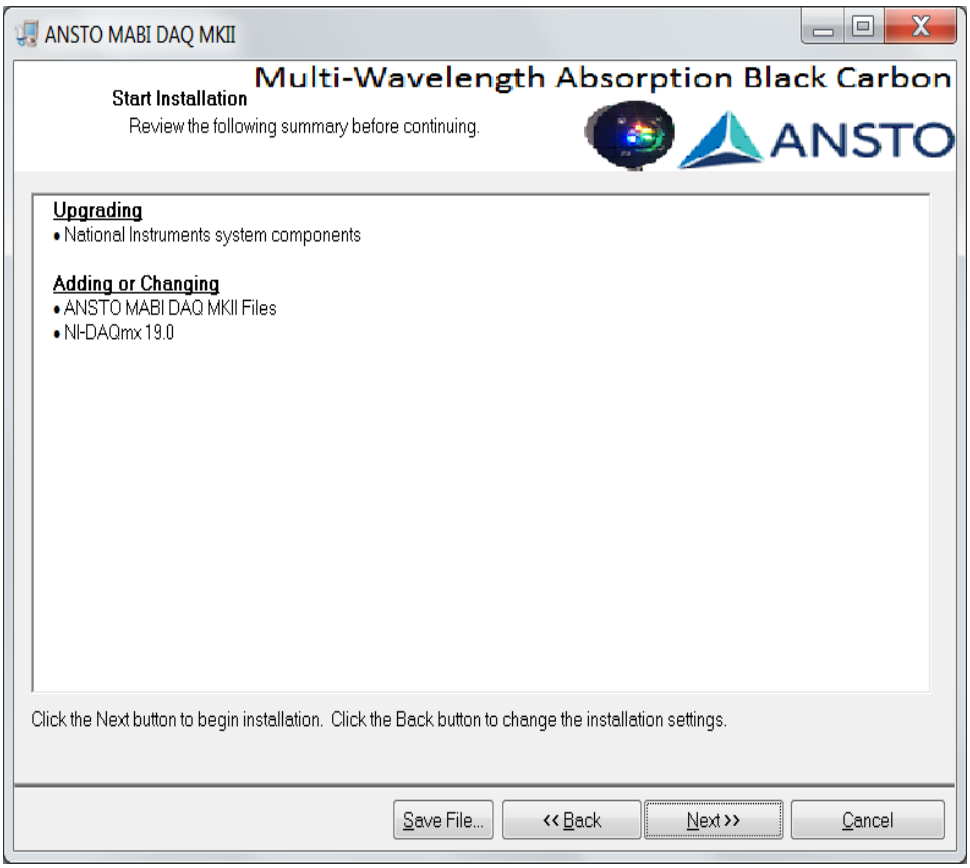

Figure 9. Image of the start installation screen.

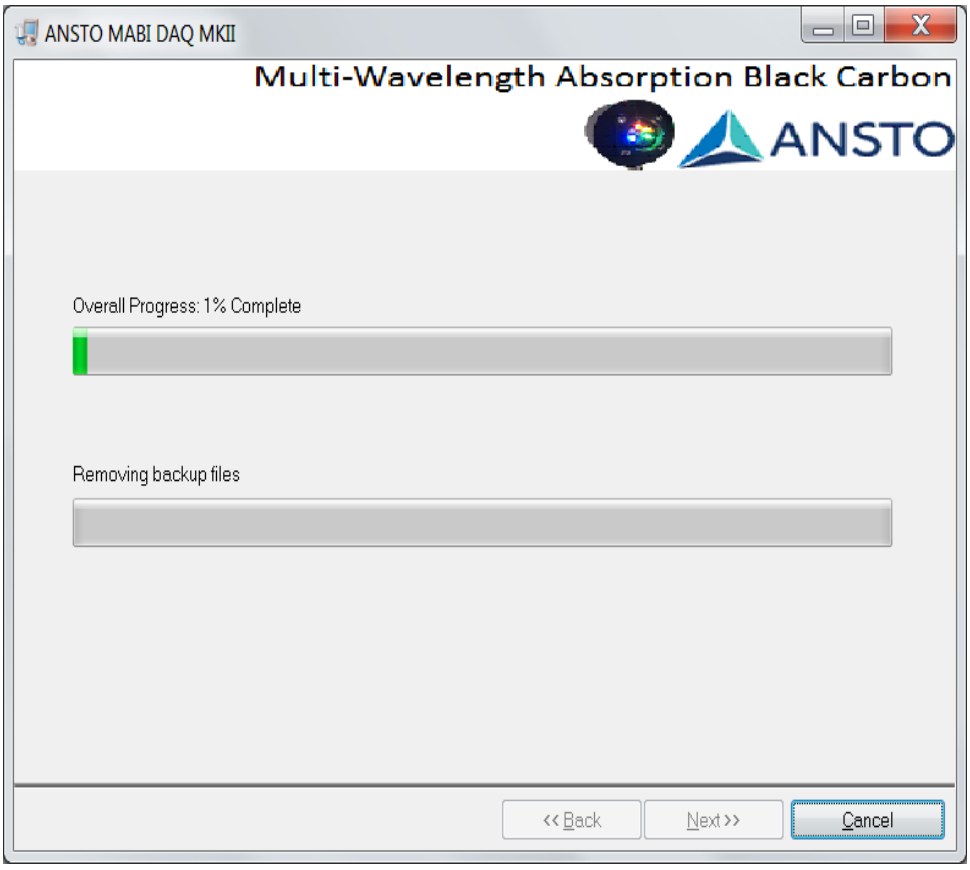

Figure 10. Image of the installation progress screen.

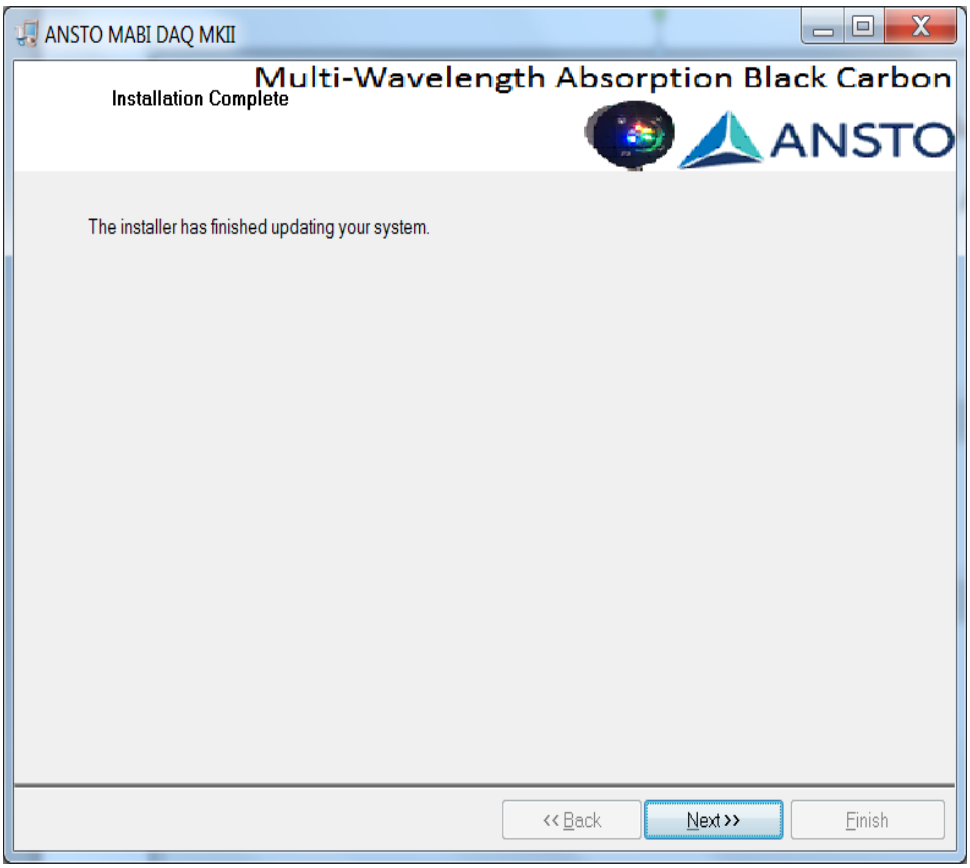

Figure 11. Image of the installation complete screen.

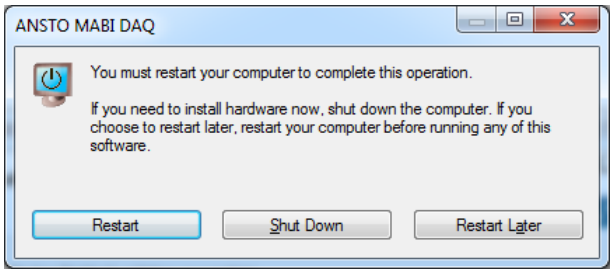

Figure 12. Image of the computer restart required screen.

Please restart your computer at this point to complete the installation process., do not attempt to run the software until the system has been restarted

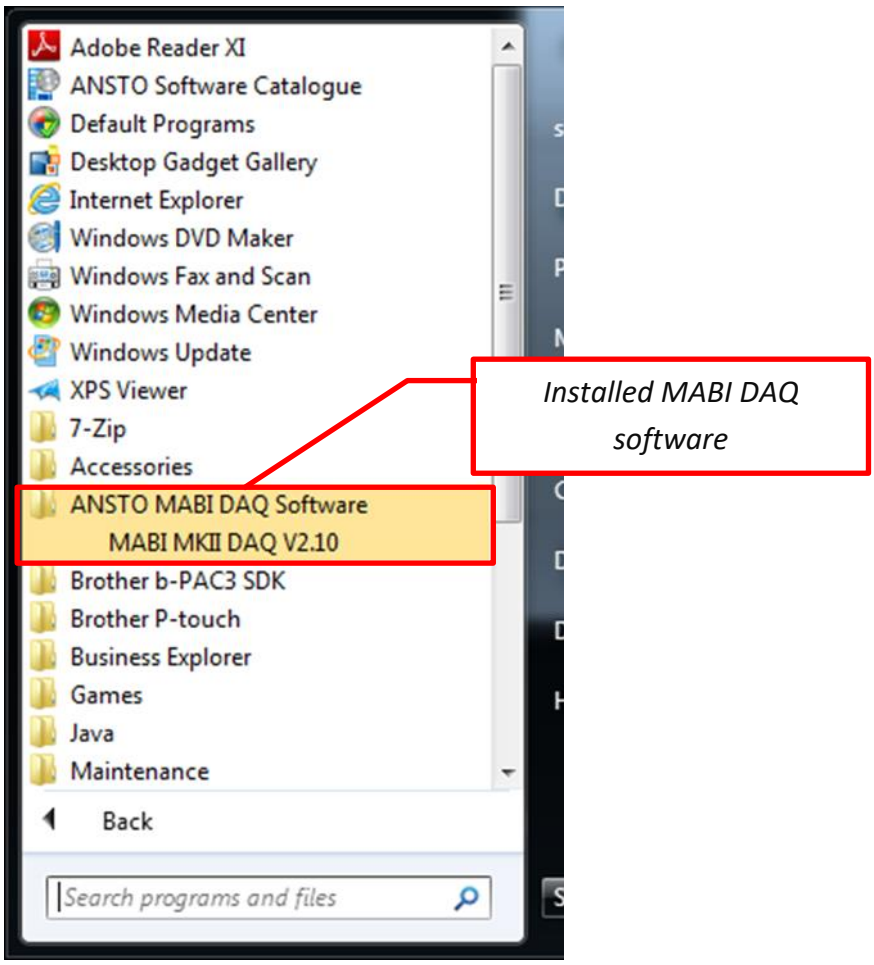

Figure 13. Image showing successful installation of the MABI DAQ software.

The MABI instrument, including hardware assembly and software installation, is now complete. The system is now ready to use. The following sections will take you through the MABI Data Acquisition (MABI DAQ) software.

ANSTO MABI DAQ Software Operation

All of the hardware and software components are now correctly assembled and installed. The following steps take you through the basic operational flow of the MABI DAQ software.

Step:

(1) Locate the MABI DAQ software program installed in the previous step and open it

(2) As part of the software opening process, the software will automatically check that all of the required hardware components are attached and powered. If it detects missing hardware, a warning message will be displayed with some basic trouble shooting

instructions (Figure 14). Double check the connections and that power has been switched on to all hardware before you press “OK” or “Ignore Warnings” to continue.

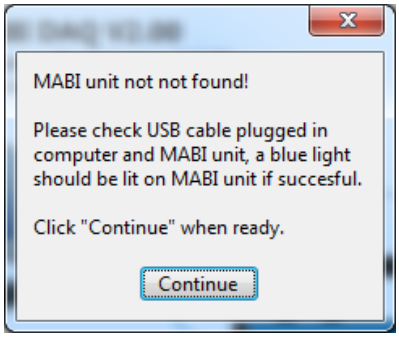

Figure 14. MABI software hardware issue and trouble-shooting message.

(2) You should now see the main MABI program screen (Figure 15). The following section explains the information shown in the various regions of the main MABI screen (marked A to F and highlighted in Figure 15).

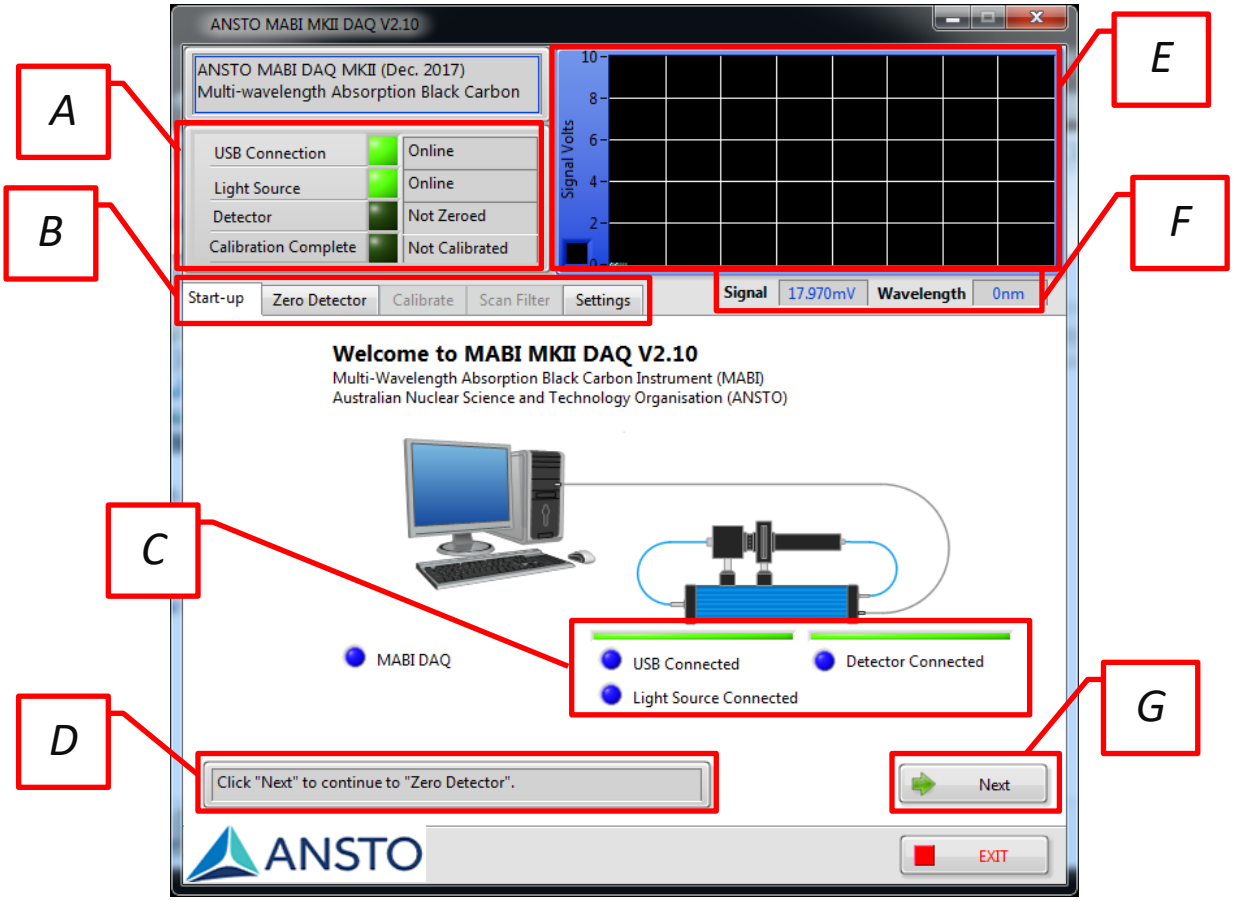

Figure 15. MABI software application main “start-up” window. The highlighted sections of this window are described in the text below.

The following text describes the highlighted sections shown in Figure 15:

A) This is used to track the completion progress of steps required to initiate and calibrate the MABI unit prior to performing the intensity measurements. The green indicator squares will successively illuminate and the adjacent text box will inform provide a comment such as “Online”, Detector Zeroed” or “Calibrated” as each step is successfully completed. When the software is opened for the first time, only the USB Connection and Light Source indicator squares should be illuminated to denote that the hardware is correctly attached and powered.

B) This section provides the tabs for navigating the different function screens in the MABI DAQ software. Clicking on the tab will take you to that screen. On the initial software start-up, the Calibrate and Scan Filter tab are greyed out and not selectable until the Zero-Detector tab has been completed.

C) This section is used to visually represent, with a green coloured bar, that the associated hardware component is correctly attached and active. All bars should be illuminated green. If a component in this section has a red coloured bar, please check the hardware components listed under the red bar are correctly installed and switched on. The software automatically and continuously checks these components. If you are unable to correct an issue, please contact the MABI DAQ Support Team.

D) This is the main instructional dialogue box on the user interface and should be referred to often during each of the following steps. It provides the user with procedural information such as what step to perform next, to wait if a function is in progress or confirmation when a process has completed.

E) This is a real time chart of the detected signal voltage.

F) These information boxes inform the user of the real-time voltage and the activated LED wavelength in nm.

4) If the first two indicator lights in section A (**Figure 15**) and all indicator bars in section C (**Figure 15**) are green, you can now zero the detector by pressing the “Next” button (**Figure 15 - G**) which will take you to the Zero Detector page shown in **Figure 16**. Press the green Zero Detector button (**Figure 16**)**.**

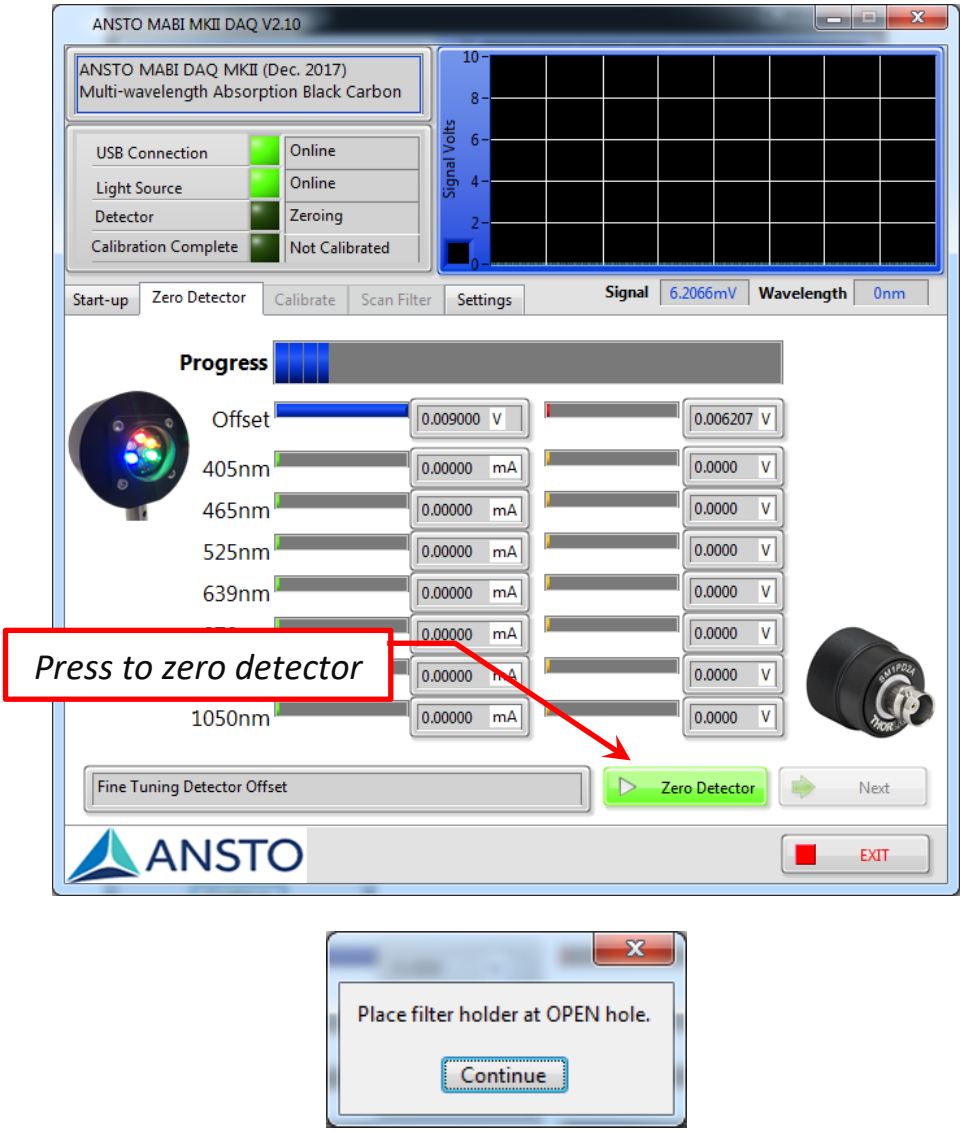

Figure 16. MABI application "zero detector" screen and the reminder notice to move the filter holder to the OPEN hole position before performing the calibration.

Before the zeroing process begins, you will be instructed to place the filter holder to the empty "OPEN" hole position (**Figure 16**). The detector zeroing process will start automatically and its progress shown on the on-screen progress bar.

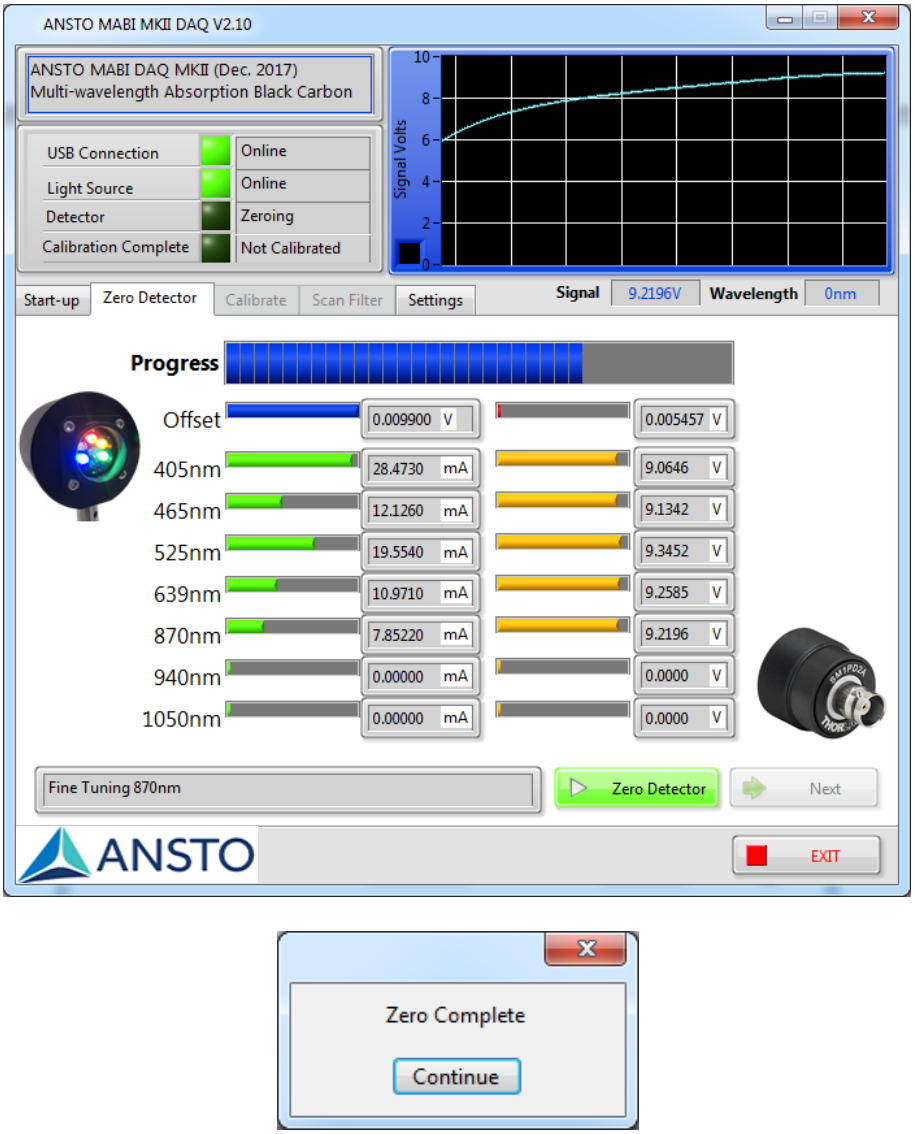

Figure 17. Zero detection calibration in progress window and zero complete window.

The detector has now been calibrated and zeroed (**Figure 17**).

5) Press “Next” to continue to perform the light source calibration. This will take you to the Calibrate page. A pop-up box will instruct you to move the holder to the open hole position (**Figure 19**) i.e. align the holder to a position that does NOT contain a filter (i.e. open hole) in order for maximum light transmission at each wavelength to the detector during calibration. It is recommended that the last position of each holder is left empty (i.e. open hole) for regular calibration purposes. If this process is followed, the schematic diagram in **Figure 21** illustrates how to align the holder to the empty open hole as the last position of the holder.

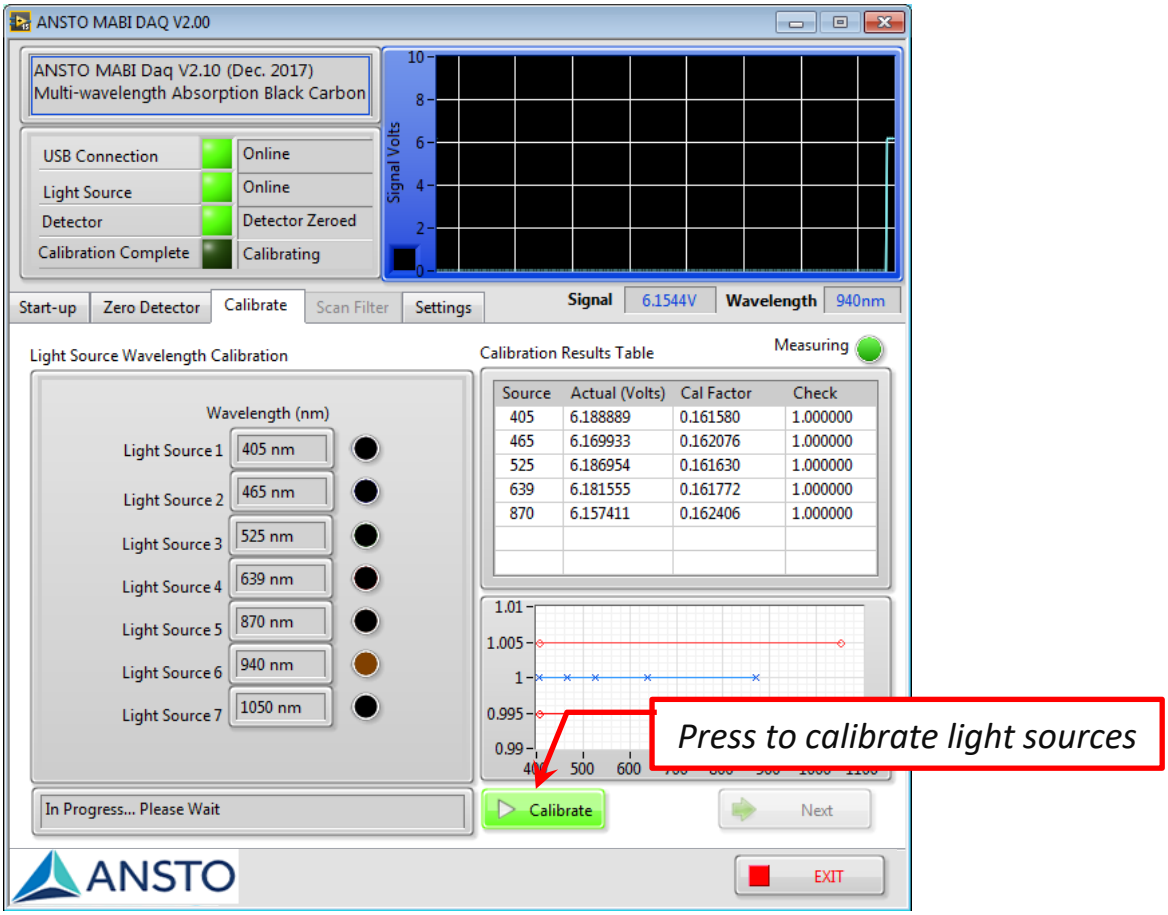

Figure 18. MABI application calibrate window.

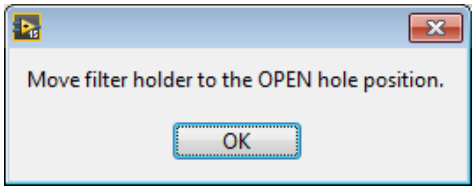

Figure 19. MABI application pop-up window informing user to align the sample holder to an open hole (i.e. empty) position.

Once the filter holder is aligned to the OPEN hole position, press the green “Calibrate” button (Figure 18).

Figure 20. These pictures show the correct alignment of position 1 marker on the 25mm diameter filter holder with the sample holder edge. Similar alignment can be performed for position markers 2 to 8.Note: there is an orientation channel on the bottom edge of each filter holder to ensure the filter holder can only be inserted in the correct orientation. Ball detent notches along the orientation channel also provide physical feedback as each filter position is correctly aligned during holder insertion.

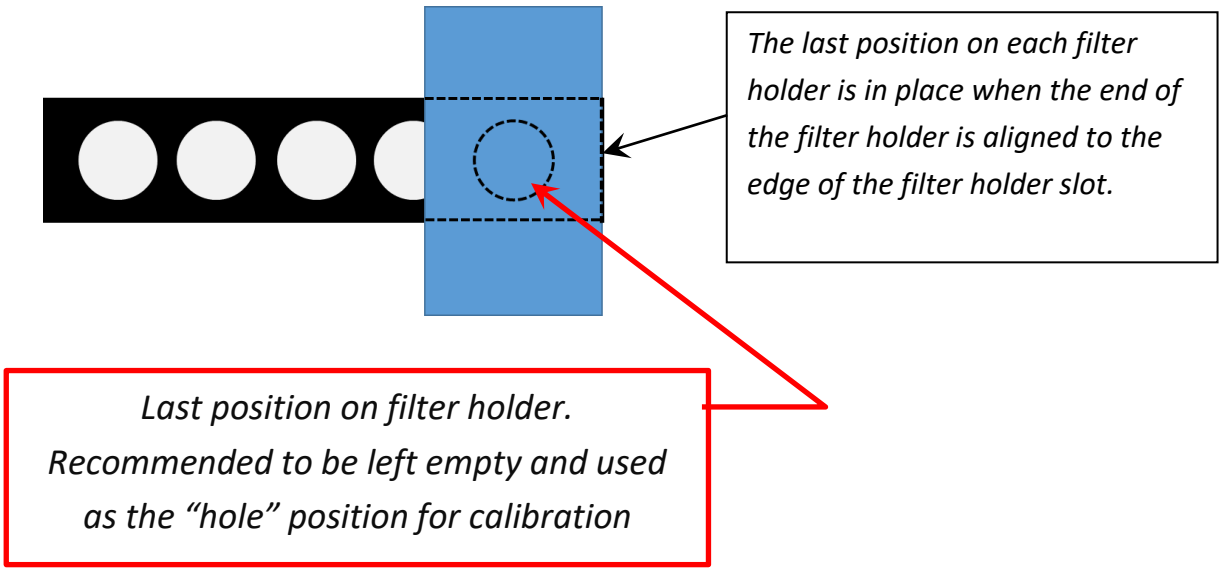

Figure 21. Schematic diagram showing the sample holder slot notch alignment required for the last filter position on the holder. Note: All other filter positions on the holder are aligned by lining up the position markers etched on the top of the holder with the inner edge of the sample holder slot notch as shown in Figure 20.

The calibrate process will now automatically run through twice. The progress through each LED is shown by the circular indicator next to each light source number which will illuminate when each LED is activated (Figure 22). After each LED, the resulting calibration values will be presented in the calibration table and chart (Figure 22). During the first calibration cycle, the "Check" column and the chart will show a value of exactly "1" for each LED as the

system is adjusting the maximum transmission power for each LED to be 1 (unity). During the second calibration cycle, the system uses the adjustment values generated during the first calibration cycle to measure actual transmission readings. At the completion of the second calibration cycle, the "check" column values should be within 1.000 ± 0.005. This tolerance is marked on the chart with red tramlines.

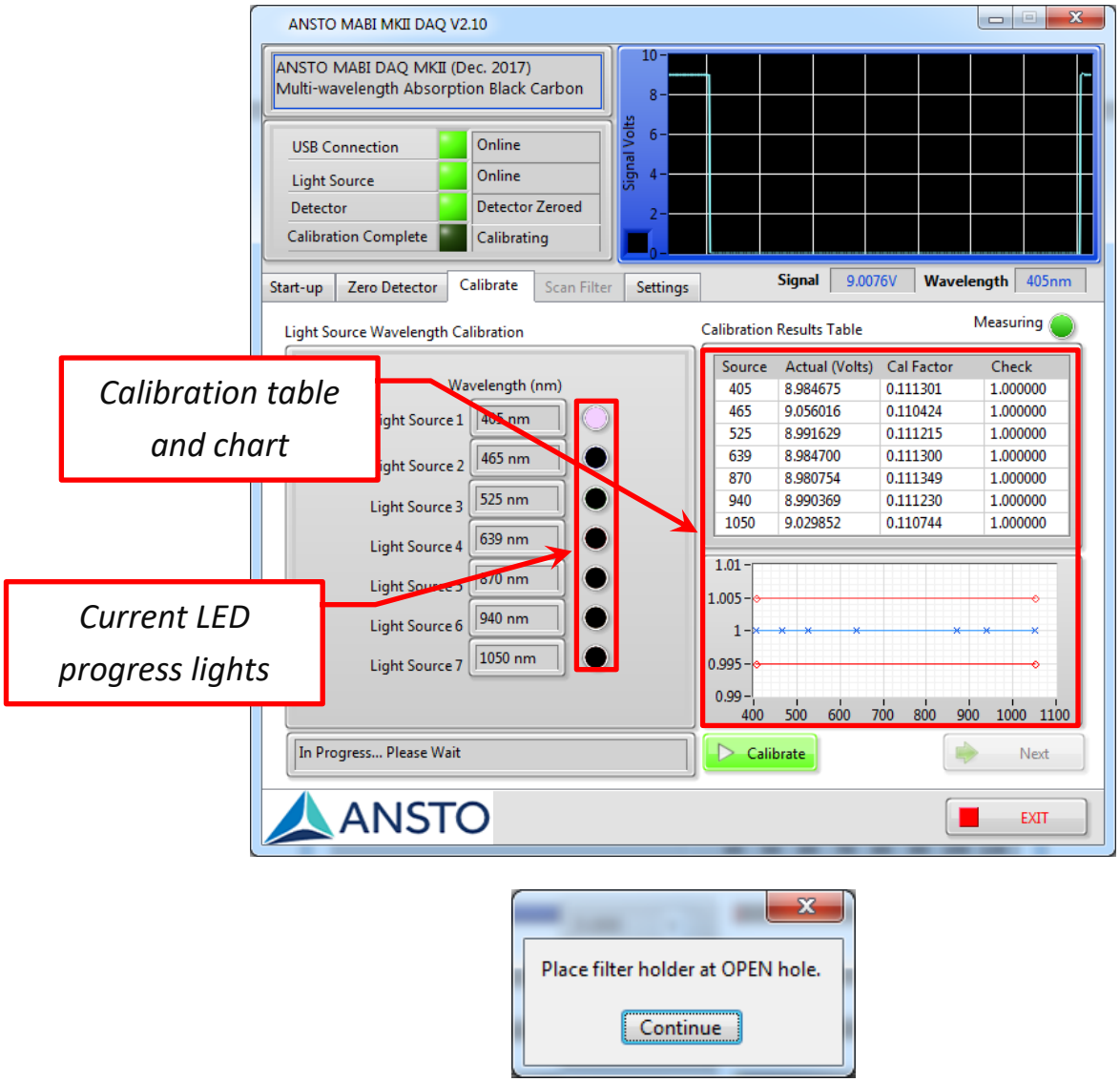

Figure 22. MABI application "calibrate" screen showing the first calibration cycle in progress.

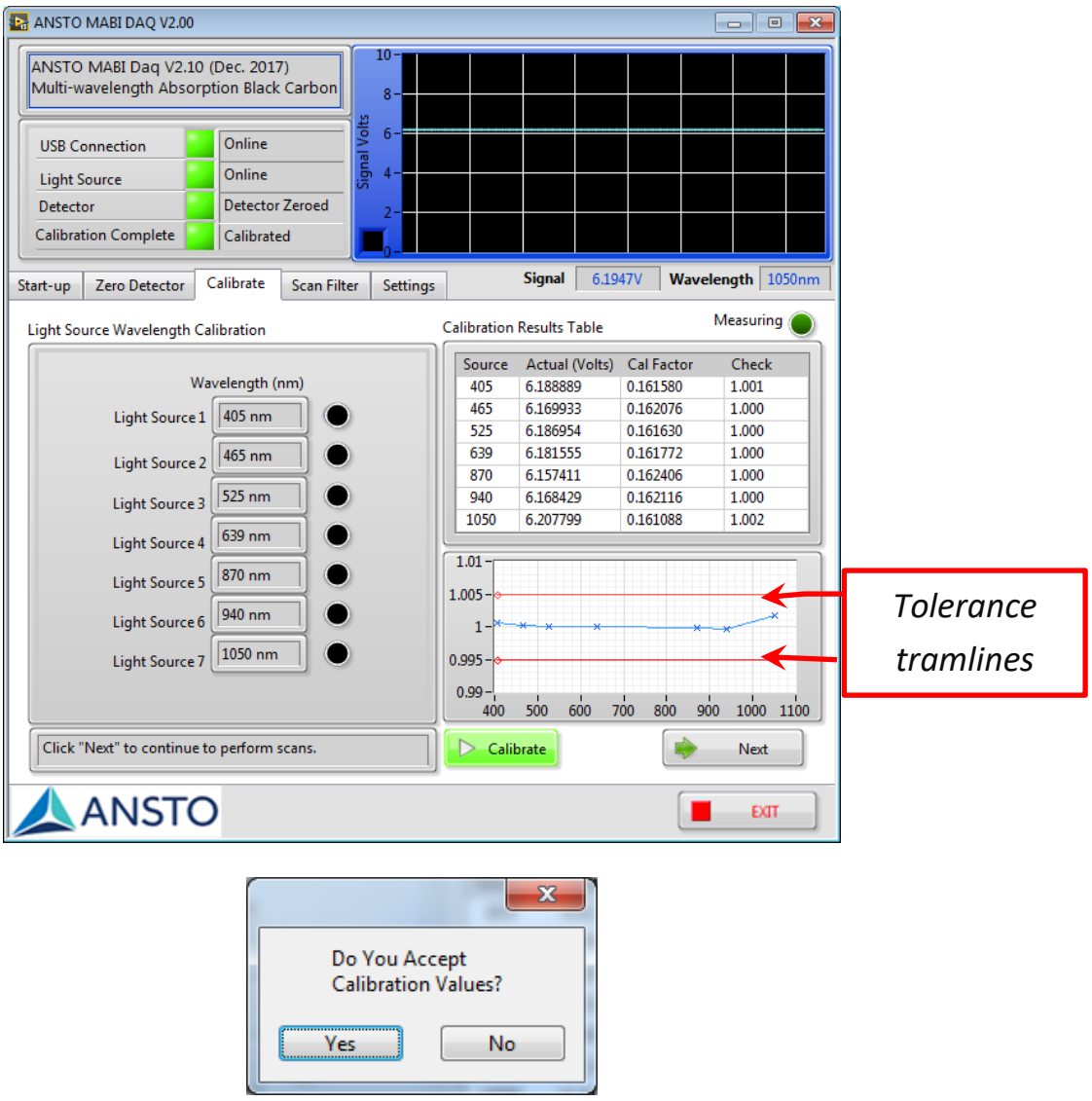

Figure 23. MABI application "calibrate" screen at the completion of the second calibration cycle. The calibration chart provides a visual representation of whether all wavelengths are within the ±0.005 tolerance tramlines. If so, you can "Accept" the calibration values and continue to take MABI measurements on actual filters. If not, press "No" to reject the calibration and repeat the process.

Additional MABI Software Settings

The “Settings” page provides a number of settings that can be adjusted by the user if required (**Figure 24**). These include modifying the wavelength value of each LED. Changing the default path where the data output file will be saved. Changing the stabilisation delay performed at each wavelength to ensure adequate reading stability is achieved before taking a measurement. A value of 2 or 3 seconds is recommended.

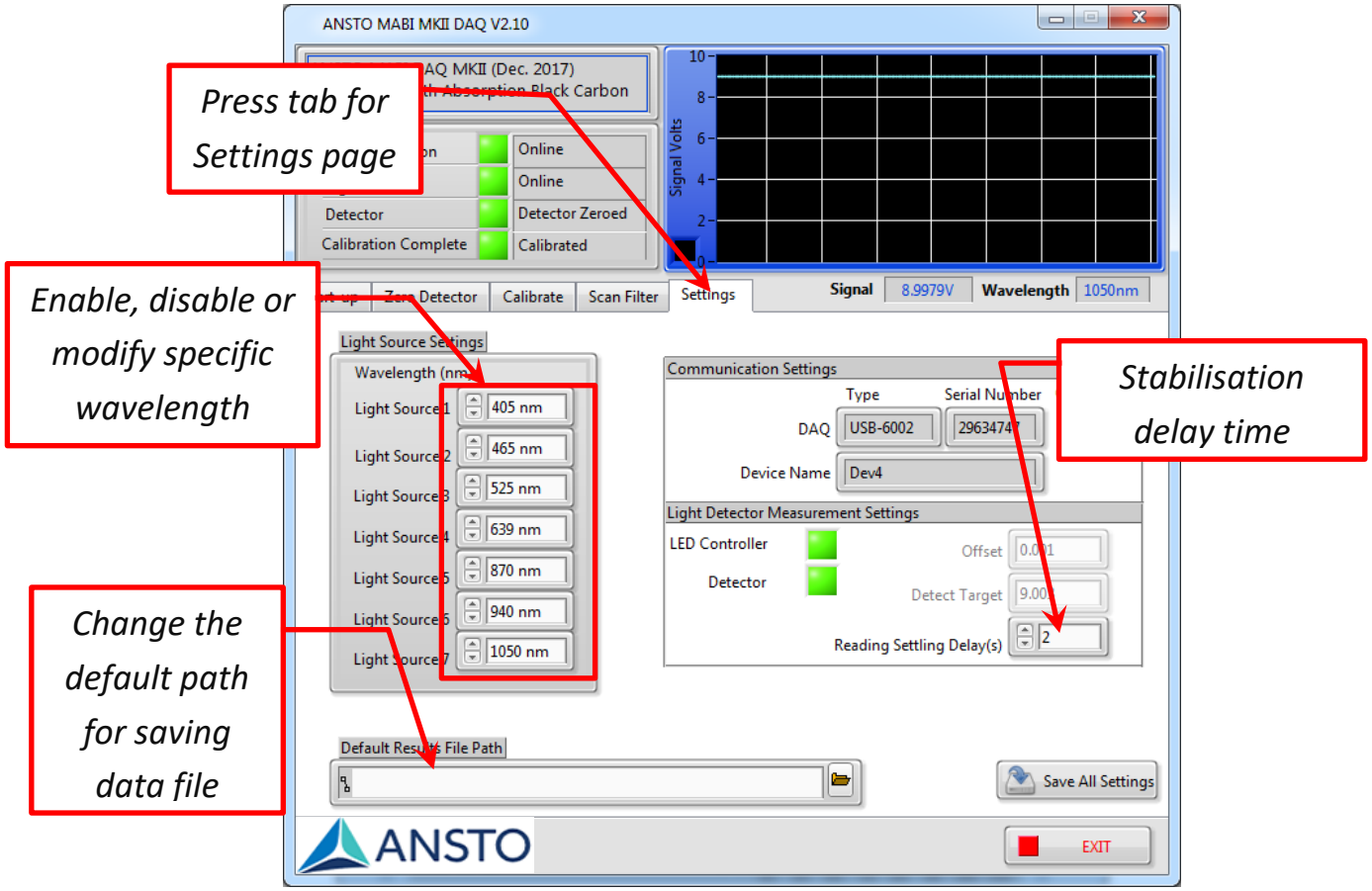

Figure 24. MABI application setting screen.

MABI Filter Analysis Example

Now that your instrument is fully and correctly assembled, initialised and configured, the following section details how to insert a sample and acquire your first set of data.

Loading Samples in Sample Holders

Two types of sample holders are provided. These are holders designed to accommodate a 25mm and 47mm filter as seen in Figure 25 and Figure 26, respectively. The 25mm holder type can load a maximum of 6 filters and the 47mm type can load 4. The 47mm filter can also accommodate a 37mm filter if required.

Sample Holder Description and Key Components

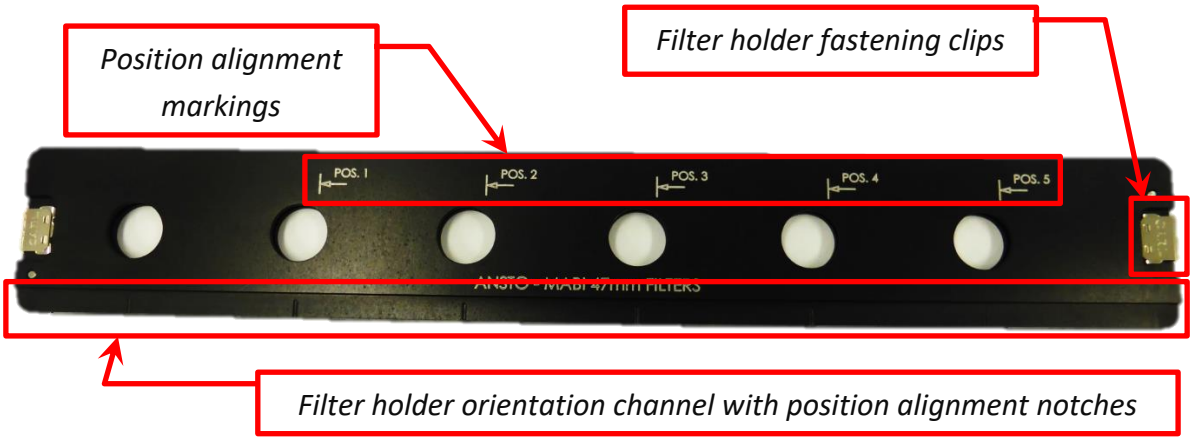

Figure 25. Image showing the position alignment markings along top of 25mm sample holder and the fastening clips used to hold the two sections of the filter holder together. Each filter holder also has an orientation groove to ensure it cannot be inserted incorrectly into the sample holder slot on the MABI.

Each Sample holder assembly is comprised of two components: a top and bottom section. The sample alignment positions are marked on the outside of the top section from left to right. **NOTE: these markings are used to align the sample holder with the sample holder slot (shown in Figure 20) and are NOT labels of the filter positions on the sample holder itself. The actual sample positions are labelled on the inside of the top section left to right as shown in Figure 26.** It is recommended that the last position of each holder is kept empty so that it can be used as the "OPEN" empty hole position required for performing the calibration scan (see **Figure 22** and **Figure 23** and associated text).

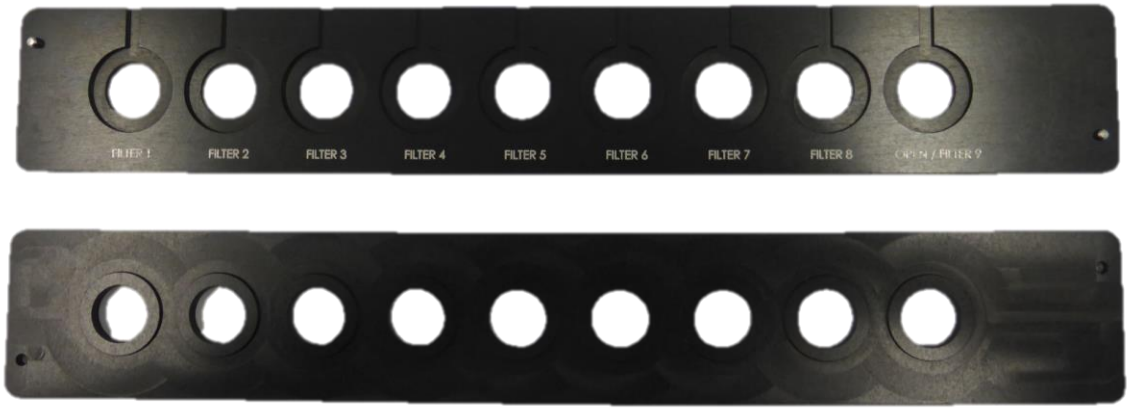

Figure 26. Image of the inside of the sample holder. The top image shows the recessed grooves where the 25mm filters should be placed with the exposed side facing up. Each position is labelled with FILTER 1-6, with the final position also labelled "OPEN" as this position is recommended to be left empty and used for regular calibration purposes.

These top and bottom components are held together using two quick release push-pull spring clips as shown in Figure 28. **Important note: Before pushing the clips on to each end of the sample holder, ensure the internal 3-tooth spring section is extended by gently pulling the components apart with your fingers as shown in Figure 27**. To remove the clip, simply pull it out in the reverse direction to the installation.

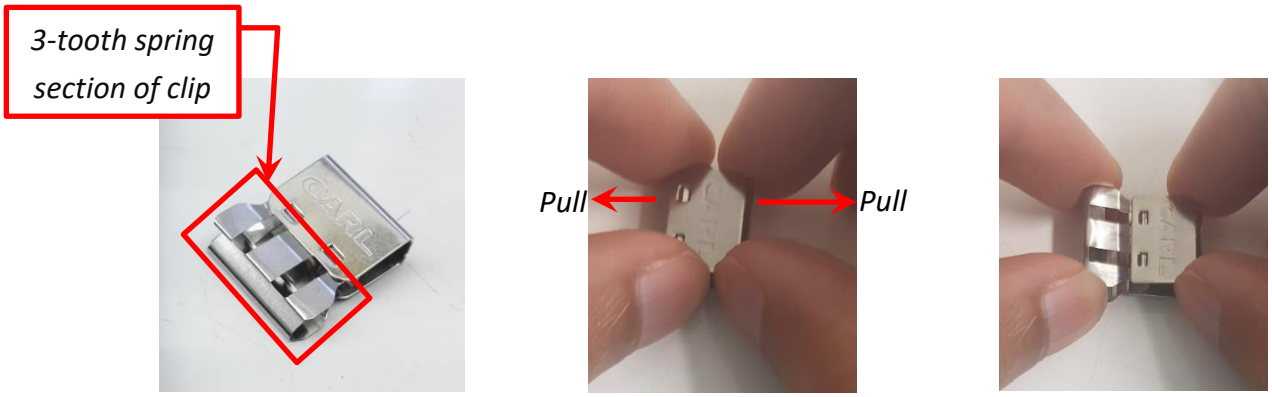

Figure 27. Image of the quick release push-pull spring clip and how to extend 3-tooth spring section of clip before use on sample holder

Figure 28. Image showing the use of the spring clip to secure the two components of the sample holder together.

Load a set of unexposed filters to perform the I_o measurements. Ensure each filter is laid fully inside the filter-groove section correctly to prevent damage. **Ensure filters are always oriented exposure side up for correct measurements**.

Place bottom section of holder onto the top section (where the filters where laid) and clip the two holder components together to secure the sample holder assembly.

Insert and Position Filter Holder in MABI

Insert the assembled sample holder into the MABI holder slot with the top component of the sample holder (i.e. component with position markings) on the same side as the sample slot notch as show in **Figure 20**.

Use the filter position markings printed along the top edge of the top component of the sample holder to align with the edge of the sample slot notch as shown in **Figure 20**.

Our recommendation is that the last position of each sample holder should be left empty or "OPEN" (i.e. without any filter loaded) and used for performing the regular calibration scan at the end of each full filter holder of measurements to ensure the photo-detector hasn't drifted.

Move the sample holder to the last position by aligning the sample holder edge with the internal edge of the thumb notch on the sample holder slot. This alignment is shown schematically in **Figure 21**.

Calibration

Perform the pre-scan calibration at this "OPEN" (hole) position as shown earlier in **Figure 22** and **Figure 23** and described in associated text. It is recommended that this calibration is being checked at regular intervals during the measurement of multiple holders to re-calibrate for any drift which can occur over extended periods. Ideally, this should be done at the end of each holder using the "Hole Scan" button described later on the "Scan Filter" page.

Press the "Next" button on the calibration screen once the calibration has finished (**Figure 23**). This will take you to the "Scan Filter" page as shown in **Figure 30**.

Figure 29. Image of the filter holder correctly aligned to position 1 (POS. 1).

Performing a Filter Scan

The following steps can now be performed to acquire data for each filter loaded in the sample holder. Load filters into all positions on the filter holder except the last position which should be left empty. Close and secure the sample holder using the clips.

If the aligned filter in position 1 is an unexposed (blank) filter, press the "Blank Filter" button (**Figure 30**). Alternatively, if the aligned filter in position 1 is an exposed filter, press the "Exposed Filter" button (Figure 30).

After pressing either button, wait until the MABI data for each wavelength is displayed in the data table before moving to the next filter.

Repeat this process, moving the filter holder to each position successively, until data is collected for each occupied filter position.

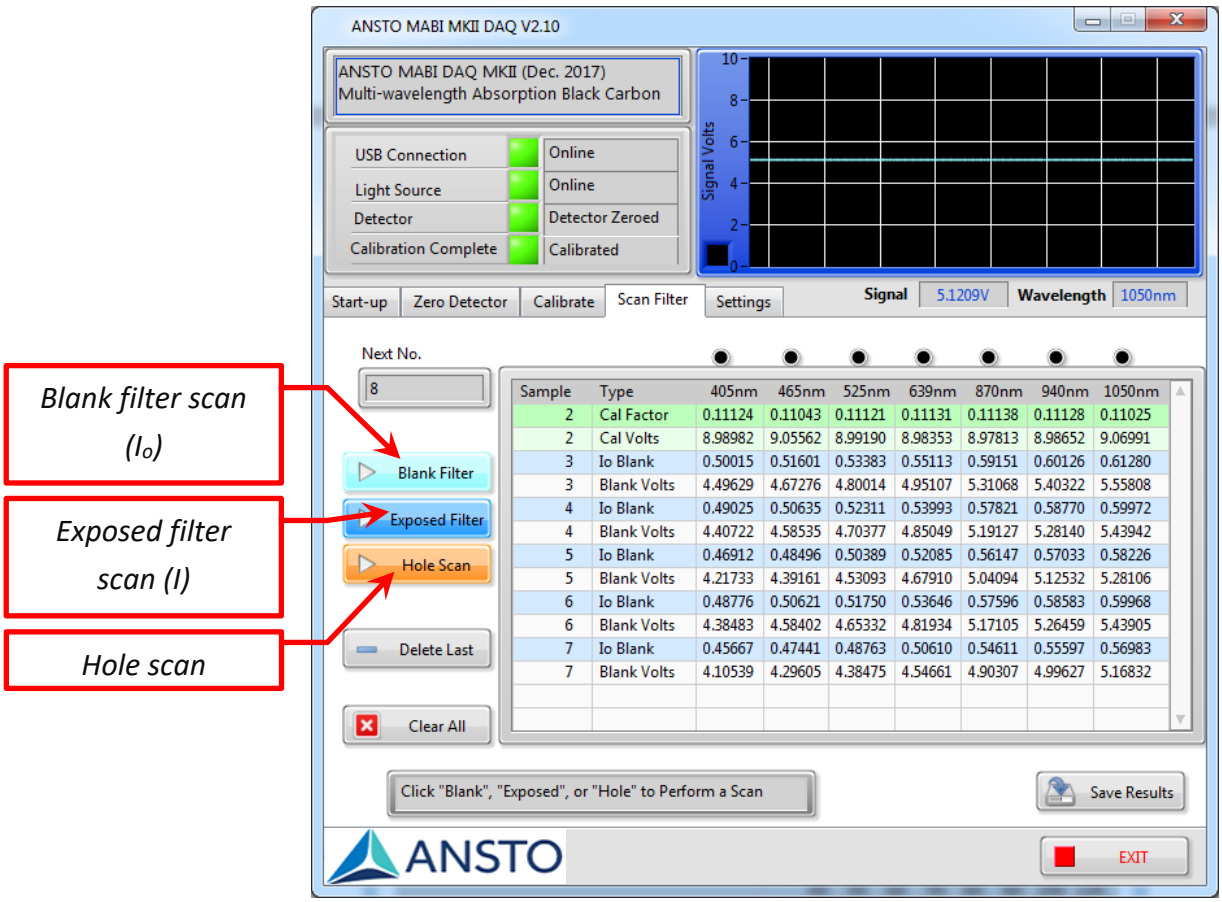

Figure 30. MABI application scan filter screen.

Finally, align the filter holder to the empty ”OPEN” hole position (which should be the last position on the filter holder) and press the “Hole Scan” button. Check that the resulting open hole values in the data table are still within 1.000±0.005. If ok, you can move on to measuring the next set of filters. If not, the full calibration process should be performed again before continuing with further filter scans. For full calibration refer to **Figure 22** and **Figure 23** and the associated text.

PLEASE NOTE: The “Blank Filter”, “Exposed Filter” and “Hole Filter” buttons (shown in **Figure 30**) all effectively perform the same scan – i.e. the resulting values will be the same regardless of which scan button is pressed. The only difference is the “Type” label that the MABI software assigns to the data in the output data table. i.e. “I_0 Blank”, “I Exposed” or “Hole”. The Hole scan will also update the calibration plot shown on the Calibrate window which can be viewed after the Hole scan is completed by selecting the Calibrate tab.

The “Delete Last” button can be used to delete only the last row of data from the data table. This button can be used multiple times if you wish to remove several rows of data.

Data Table

The following describes the data presented in the data table.

For each scan, whether "Blank Filter", "Exposed Filter" or "Hole Scan", two rows of associated data will appear in the data table. The first data row provides the values measured at each wavelength and adjusted by a calibration factor determined for each LED during the calibration process. These are the values you should use for subsequent black carbon calculations. The second data row provides the raw voltage (V) values measured at each wavelength without the calibration factor applied. This second row of data is provided for measurement transparency and data completeness only. This second data row for each scan is easily identified in the data table as it will include the word "Volts" in the "Type" column shown in **Figure 31**.

An example of the various two row data outputs for each scan is shown below (**Figure 31**)

Two data rows per scan (calibrated and actual)

Sample	Type	405nm	465nm	525nm	639nm	870nm	940nm	1050nm
2	Cal Factor	0.11124	0.11043	0.11121	0.11131	0.11138	0.11128	0.11025
2	Cal Volts	8.98982	9.05562	8.99190	8.98353	8.97813	8.98652	9.06991
3	Io Blank	0.50015	0.51601	0.53383	0.55113	0.59151	0.60126	0.61280
3	Blank Volts	4.49629	4.67276	4.80014	4.95107	5.31068	5.40322	5.55808
4	Io Blank	0.49025	0.50635	0.52311	0.53993	0.57821	0.58770	0.59972
4	Blank Volts	4.40722	4.58535	4.70377	4.85049	5.19127	5.28140	5.43942
5	Io Blank	0.46912	0.48496	0.50389	0.52085	0.56147	0.57033	0.58226
5	Blank Volts	4.21733	4.39161	4.53093	4.67910	5.04094	5.12532	5.28106
6	Io Blank	0.48776	0.50621	0.51750	0.53646	0.57596	0.58583	0.59968
6	Blank Volts	4.38483	4.58402	4.65332	4.81934	5.17105	5.26459	5.43905
7	Io Blank	0.45667	0.47441	0.48763	0.50610	0.54611	0.55597	0.56983
7	Blank Volts	4.10539	4.29605	4.38475	4.54661	4.90307	4.99627	5.16832

Figure 31. Example of the two data rows generated from each scan.

Saving the Data to Associated .csv File

The data in the data table can be saved to a results file (.csv) by pressing the "Save results" button (**Figure 32**) which generates an output file of the data in .csv format and saves it to the path location specified in the "Settings" screen. An example of the actual Scan Filter window is shown in **Figure 34** after the following filter scan sequence was performed:

1) Sample 2 = OPEN hole scan on the last (empty) position on the filter holder performed on the Calibrate window

2) Sample 3 = Blank filter scan located in position 1 on the filter holder

3) Sample 4 = Blank filter scan located in position 2 on the filter holder

4) Sample 5 = Blank filter scan located in position 3 on the filter holder

5) Sample 6 = Blank filter scan located in position 4 on the filter holder

6) Sample 7 = Blank filter scan located in position 5 on the filter holder

7) Sample 8 = Hole Scan located in position 6 (last position) on the filter holder performed as a regular calibration check before accepting the 5 previous filter scans

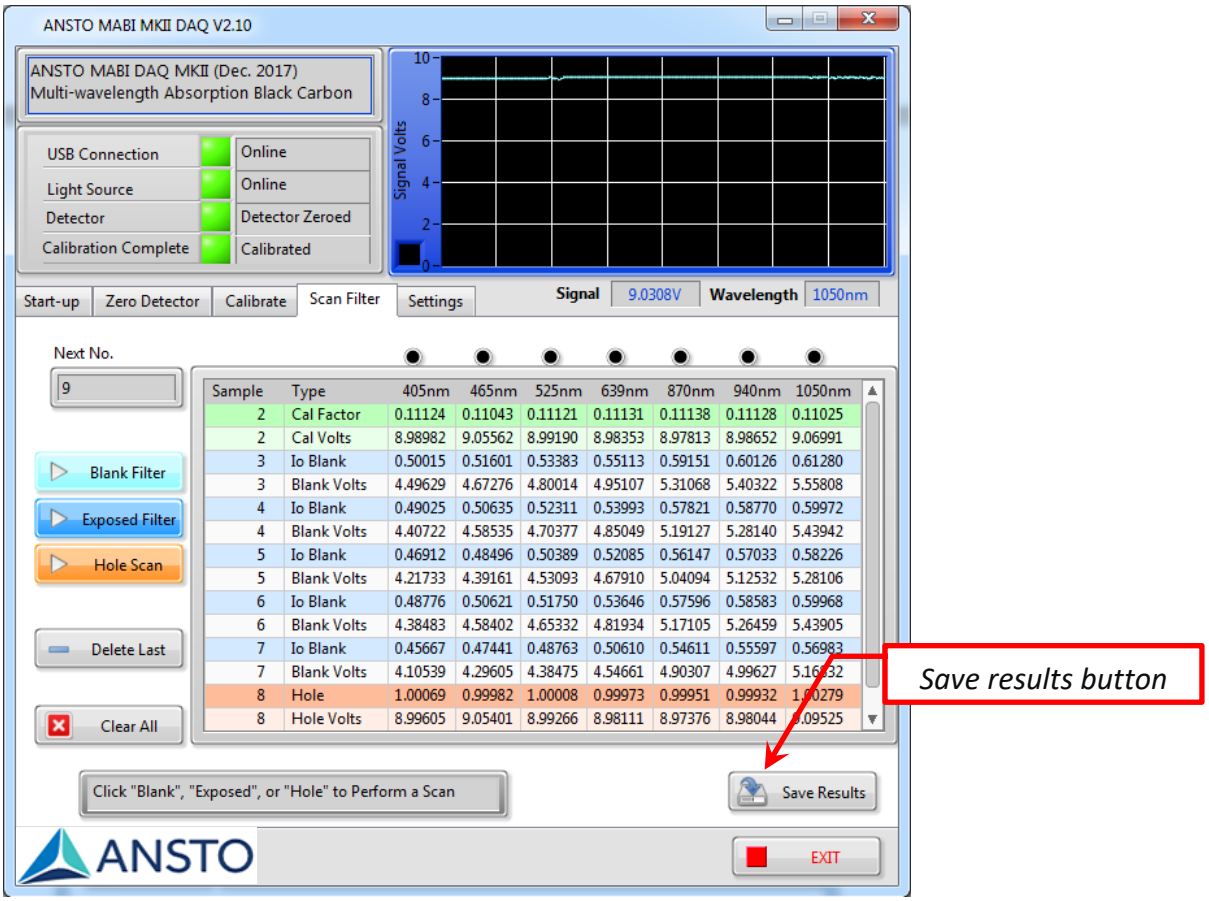

Figure 32. MABI application Scan Filter screen showing the location of the save results button.

After the Hole scan, press the Calibrate tab to check if all wavelengths in the associated OPEN hole calibration plot are within the tramlines (**Figure 33**). If not, then re-calibrate the wavelengths and repeat the scans for all filters on that filter holder. If the OPEN hole calibration are within the tramlines, you can move on to the next set of filter scans or save the data file by returning to the Scan Filter tab and pressing the Save Results button.

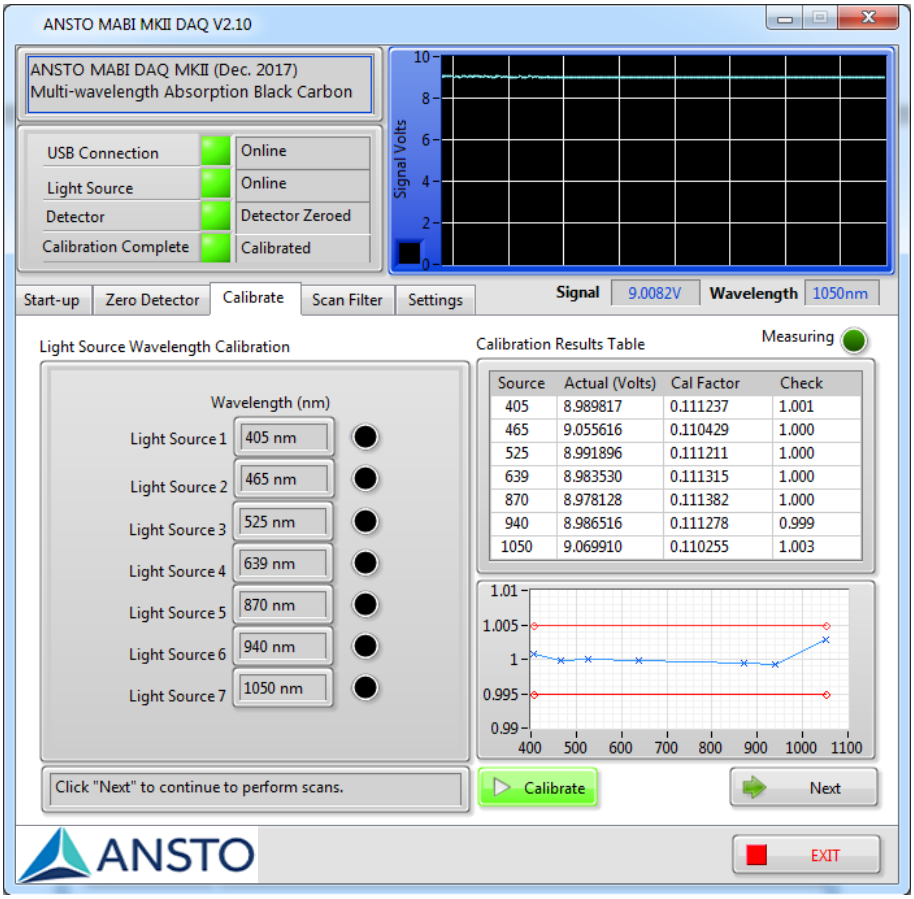

Figure 33. MABI application Calibrate window which has been updated after an OPEN hole scan is performed on the Scan Filter window.

Pressing the Save Results button on the Scan Filter windows will save the data as a .csv file to a chosen location on your computer. The format of that output file (example shown in **Figure 34**) is slightly different to what is presented in the MABI application Scan Filter window during measurement. While the two rows of data described above (Calibrated and raw Volts) for each scan are provided, they have been separated so that all of the raw Volts data and data related to calibration (i.e. scans performed on the Calibrate window and Hole scans performed on the Scan Filter window) are grouped at the top of file while the "I_o Blank" and "I Exposed" data required for subsequent calculations are grouped below in the "Intensity Results" section. This was done to make it easier for the user to select/copy all of the I_0 or I values from the "Intensity Results" section in order to perform the b_{abs} or BC calculations. Despite this separation, it is important to note that the "Sample number" and the "Date Time Stamp" for the two related data rows of each scan remain correlated, as shown in **Figure 34** using sample 1 and sample 2 as an example.

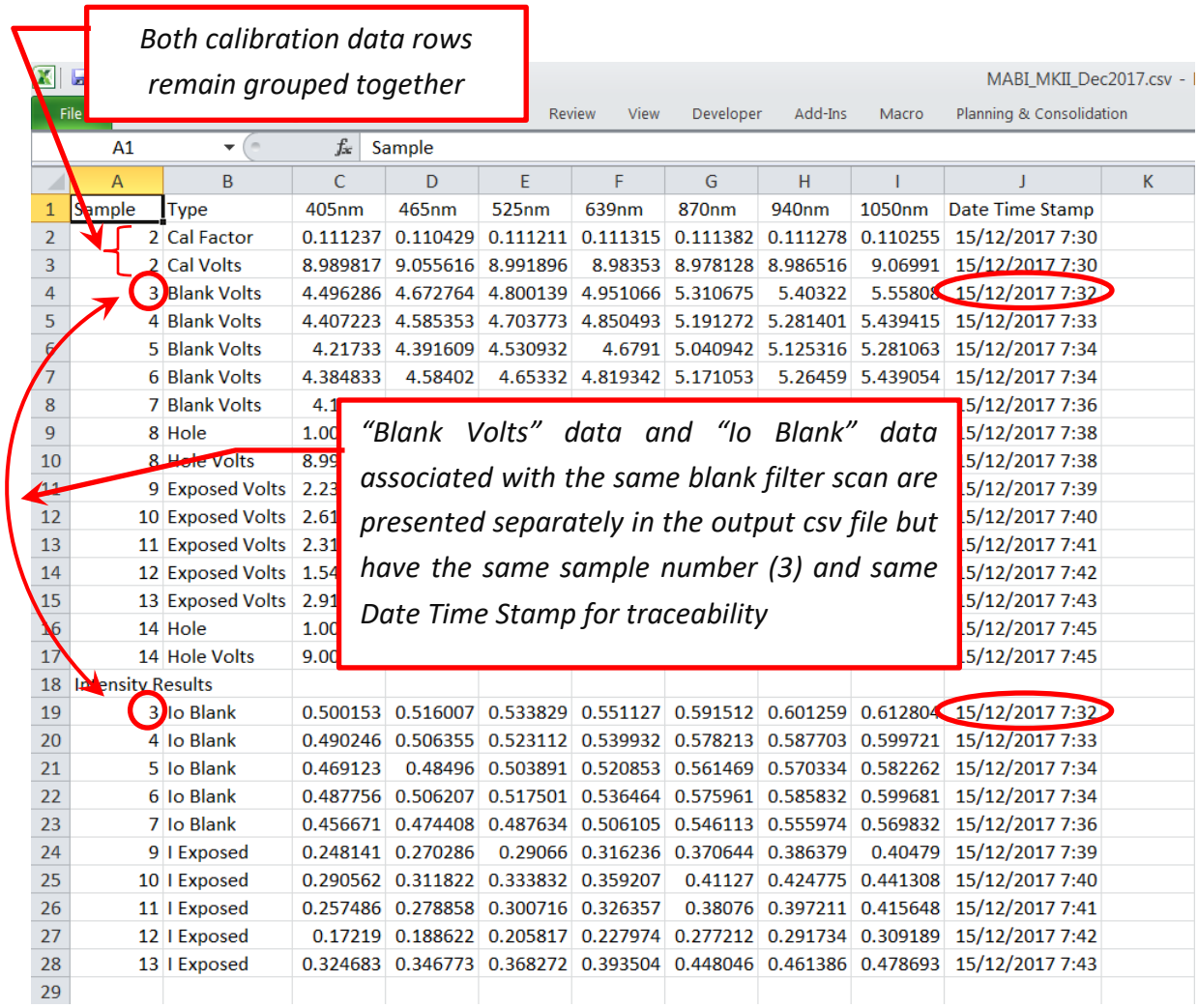

MABI_MKII_Dec2017.csv

File Review View Developer Add-Ins Macro Planning & Consolidation

A1 Sample

	A	B	C	D	E	F	G	H	I	J	K
1	Sample	Type	405nm	465nm	525nm	639nm	870nm	940nm	1050nm	Date Time Stamp	
2	2	Cal Factor	0.111237	0.110429	0.111211	0.111315	0.111382	0.111278	0.110255	15/12/2017 7:30	
3	2	Cal Volts	8.989817	9.055616	8.991896	8.98353	8.978128	8.986516	9.06991	15/12/2017 7:30	
4	3	Blank Volts	4.496286	4.672764	4.800139	4.951066	5.310675	5.40322	5.55808	15/12/2017 7:32	
5	4	Blank Volts	4.407223	4.585353	4.703773	4.850493	5.191272	5.281401	5.439415	15/12/2017 7:33	
6	5	Blank Volts	4.21733	4.391609	4.530932	4.6791	5.040942	5.125316	5.281063	15/12/2017 7:34	
7	6	Blank Volts	4.384833	4.58402	4.65332	4.819342	5.171053	5.26459	5.439054	15/12/2017 7:34	
8	7	Blank Volts	4.1							5/12/2017 7:36	
9	8	Hole	1.00							5/12/2017 7:38	
10	8	Hole Volts	8.99							5/12/2017 7:38	
11	9	Exposed Volts	2.23							5/12/2017 7:39	
12	10	Exposed Volts	2.61							5/12/2017 7:40	
13	11	Exposed Volts	2.31							5/12/2017 7:41	
14	12	Exposed Volts	1.54							5/12/2017 7:42	
15	13	Exposed Volts	2.91							5/12/2017 7:43	
16	14	Hole	1.00							5/12/2017 7:45	
17	14	Hole Volts	9.00							5/12/2017 7:45	
18	Intensity Results										
19	3	Io Blank	0.500153	0.516007	0.533829	0.551127	0.591512	0.601259	0.612804	15/12/2017 7:32	
20	4	Io Blank	0.490246	0.506355	0.523112	0.539932	0.578213	0.587703	0.599721	15/12/2017 7:33	
21	5	Io Blank	0.469123	0.48496	0.503891	0.520853	0.561469	0.570334	0.582262	15/12/2017 7:34	
22	6	Io Blank	0.487756	0.506207	0.517501	0.536464	0.575961	0.585832	0.599681	15/12/2017 7:34	
23	7	Io Blank	0.456671	0.474408	0.487634	0.506105	0.546113	0.555974	0.569832	15/12/2017 7:36	
24	9	I Exposed	0.248141	0.270286	0.29066	0.316236	0.370644	0.386379	0.40479	15/12/2017 7:39	
25	10	I Exposed	0.290562	0.311822	0.333832	0.359207	0.41127	0.424775	0.441308	15/12/2017 7:40	
26	11	I Exposed	0.257486	0.278858	0.300716	0.326357	0.38076	0.397211	0.415648	15/12/2017 7:41	
27	12	I Exposed	0.17219	0.188622	0.205817	0.227974	0.277212	0.291734	0.309189	15/12/2017 7:42	
28	13	I Exposed	0.324683	0.346773	0.368272	0.393504	0.448046	0.461386	0.478693	15/12/2017 7:43	
29											

Figure 34. Example of the csv. output file format showing the location of the two data rows generated from the calibration scan sample (2) and filter scan sample (3). All of the data above the "Intensity Results" line are related to raw volt and calibration measurements. All of the data below the "Intensity Results" line are the "Io' (Blank filter) and "I" (Exposed filter) data values for use in B_{abs} and BC calculations shown below.

How to Use the MABI Data

MABI scans are initially performed on unexposed "blank filters" to determine the absorption at each wavelength from the filter substrate. This data for black filters is referred to as $\mathbf{I_o}$. The MABI scans are then repeated on the same filters after exposure and the collection of particulate matter, i.e. "exposed filters" which represents the absorption at each wavelength from both the collected particles and the filter substrate. This transmission data is referred to as $\mathbf{I}$. Both of these values along with the filter area and sampled air volume can be used to determine the black carbon light absorption coefficient (b_{abs}) at each wavelength with the formula:

$$b_{abs}(Mm^{-1}) = 10^2 \left[\frac{A(cm^2)}{V(m^3)}\right] ln\left[\frac{I_0}{I}\right] \quad (1)$$

Where:

I_o is the light transmission on a blank unexposed filter

I is the transmission of light through an exposed filter

A is the collection area of the exposed filter in [cm^2]

V is the volume of sampled air on the filter in [m^3]

The black carbon (BC) mass concentration in [ng/m^3] can then be determined using a mass absorption coefficient (ε) in [m^2/g] at each wavelength with the formula:

$$BC\ (ngm^{-3}) = \frac{10^5[A(cm^2)]}{[\varepsilon(m^2g^{-1})][V(m^3)]} ln\left[\frac{I_0}{I}\right] \quad (2)$$

Mass absorption coefficient (ε) values for black carbon generally fall within the range of 4-11 m^2/g for the fine particle size fraction PM2.5 while the coarse size fraction PM2.5-10 is significantly lower between 1-2 m^2/g.

As an example, we have provided the mass absorption coefficient values currently used at ANSTO in **Figure 35**. You are welcome to utilise these values, or you can certainly apply your own mass absorption coefficient values with your measured, $\mathbf{I_0}$ and $\mathbf{I}$ (obtained using this MABI system) to Equation (1 and 2) above assuming your own known BC mass concentrations.

Table 2 to Table 4 provides an example of the results for b_{abs} and BC calculations performed using measurements obtained from MABI system on ten stretched Teflon ASP filters for the fine PM2.5 size fraction.

Table 2 provides the filter collection area values, sampled volume of air, blank $\mathbf{I_0}$ values measured on the MABI system, exposed **I** values measured on the MABI system for each of the ten filters**.**

Table 3 provides the calculated $\ln(I_0/I)$ results and calculated b_{abs} values using the input values from Table 2 and Equation (1) for each of the ten filters.

Table 4 are the BC values calculated using Equation (2) to determine from the mass absorption coefficient (ε) values provided in Table 1 and b_{abs} values in Table 3. Using the data fits shown in Figure 35, the power equations in Figure 35 and equation (3)can be used to determine the mass absorption coefficient, ε (m^2/g) at each wavelength, λ for a given filter type:

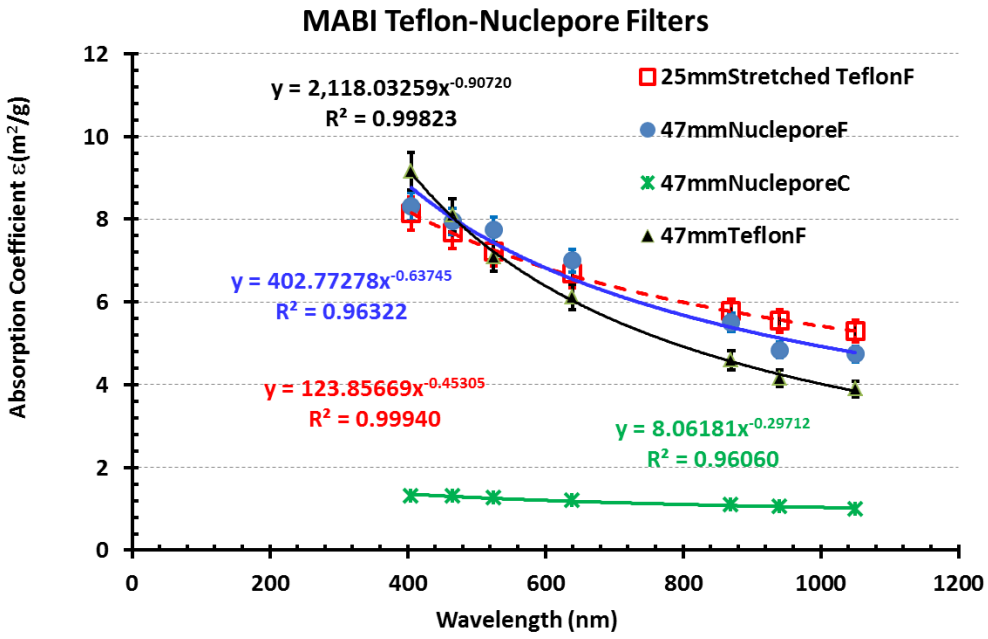

Figure 35. Plot of mass absorption coefficient (ε) versus wavelength (λ) obtained for our ASP (stretched Teflon) and GAS (Nuclepore polycarbonate) filter samples. The fitted ε values are also provided in Table 1 for each filter type and each wavelength.

Mass absorption coefficient (ε) equation as a function of wavelength (λ)is:

$$\varepsilon\ (m^2/g) = a*\lambda(nm)^b \qquad (3)$$

determined from ANSTO data fits shown in Figure 35. Where the fitted coefficients a and b are given in Table 1 for selected filter types.

Table 1. Mass Absorption Coefficient (ε) Equations as a Function of Wavelength (λ) Fitted to Equation (3)

Fitted Coefficients				
a	123.86	402.77	8.062	2118.03
b	-0.45305	-0.63745	-0.29712	-0.90720
	Mass Absorption Coefficient ε (m^2/g)			
λ(nm)	25mm Stretched Teflon (Fine PM2.5)	Polycarbonate 47mm Nuclepore (Fine PM2.5)	Polycarbonate 47mm Nuclepore Coarse PM2.5-10)	47mm Teflon (Fine PM2.5)
405	8.16	8.77	1.35	9.13
465	7.66	8.03	1.30	8.05
525	7.25	7.43	1.25	7.21
633	6.66	6.60	1.19	6.09
639	6.64	6.56	1.18	6.04
870	5.77	5.39	1.08	4.56
940	5.57	5.13	1.05	4.25
1050	5.30	4.78	1.02	3.85

Table 2. Example Data from ten ANSTO ASP Filters (25mm stretched Teflon) Including: Volume, I_0 and I Measured on the MABI System for a Filter Collection area = 2.27 cm^2

		MABI LED transmission through unexposed blank filter							MABI LED transmission through exposed filter						
ID	Vol (m^3)	I_0 (405)	I_0 (465)	I_0 (525)	I_0 (639)	I_0 (870)	I_0 (940)	I_0 (1050)	I (405)	I (465)	I (525)	I (639)	I (870)	I (940)	I (1050)
1	11.8	0.533	0.550	0.565	0.588	0.631	0.642	0.635	0.097	0.112	0.124	0.144	0.183	0.195	0.210
2	12.8	0.509	0.530	0.544	0.567	0.609	0.619	0.622	0.194	0.218	0.238	0.263	0.308	0.319	0.332
3	13.1	0.507	0.529	0.551	0.569	0.609	0.617	0.630	0.157	0.174	0.187	0.211	0.249	0.263	0.273
4	12.8	0.480	0.501	0.515	0.536	0.570	0.583	0.598	0.037	0.049	0.061	0.076	0.110	0.120	0.134
5	12.5	0.487	0.505	0.515	0.541	0.580	0.596	0.602	0.090	0.102	0.110	0.131	0.164	0.177	0.183
6	14.1	0.521	0.543	0.561	0.582	0.620	0.631	0.640	0.136	0.152	0.168	0.190	0.231	0.243	0.252
7	13.3	0.477	0.498	0.525	0.541	0.588	0.595	0.603	0.086	0.099	0.110	0.127	0.160	0.170	0.180
8	11.6	0.483	0.505	0.513	0.536	0.573	0.585	0.598	0.030	0.038	0.044	0.052	0.070	0.076	0.086
9	12.4	0.495	0.512	0.517	0.544	0.581	0.595	0.603	0.158	0.176	0.195	0.216	0.261	0.272	0.282
10	13.0	0.490	0.509	0.532	0.553	0.596	0.603	0.618	0.113	0.129	0.145	0.163	0.199	0.208	0.221

Table 3.Table Containing the Results of $\ln(I_0/I)$ and b_{abs} Calculations Performed on the data Provided in Table 4

$\ln(I_0/I)$ for each wavelength								b_{abs} (Mm^{-1}) for each wavelength						
405nm	465nm	525nm	639nm	870nm	940nm	1050nm		405nm	465nm	525nm	639nm	870nm	940nm	1050nm
1.707	1.591	1.517	1.407	1.238	1.192	1.107		32.71	30.50	29.06	26.96	23.72	22.83	21.20
0.965	0.888	0.827	0.768	0.682	0.663	0.628		17.15	15.79	14.70	13.66	12.12	11.78	11.16
1.172	1.112	1.081	0.992	0.894	0.853	0.836		20.25	19.21	18.66	17.13	15.45	14.73	14.44
2.557	2.329	2.133	1.953	1.645	1.581	1.496		45.44	41.38	37.90	34.71	29.23	28.08	26.57
1.686	1.600	1.544	1.418	1.263	1.214	1.191		30.54	28.97	27.96	25.69	22.88	21.99	21.57
1.343	1.273	1.206	1.119	0.987	0.954	0.932		21.57	20.45	19.37	17.98	15.86	15.33	14.97
1.719	1.621	1.563	1.449	1.302	1.253	1.209		29.32	27.64	26.65	24.72	22.20	21.37	20.62
2.786	2.595	2.468	2.341	2.098	2.040	1.936		54.45	50.72	48.23	45.75	41.01	39.87	37.84
1.142	1.068	0.975	0.924	0.800	0.783	0.760		20.85	19.50	17.80	16.87	14.61	14.29	13.88
1.467	1.373	1.300	1.222	1.097	1.064	1.028		25.62	23.98	22.71	21.34	19.16	18.59	17.96

Table 4. Table of Calculated Black Carbon mass Concentration values in ng/m^3 using the Mass Attenuation Coefficients given, the Data from Table3 and Equation (2)

Experimental Mass attenuation coefficients (m^2/g)						
8.14	7.68	7.23	6.69	5.78	5.55	5.30
Measured BC (µg/m^3)						
405nm	465nm	525nm	639nm	870nm	940nm	1050nm
4.02	3.97	4.02	4.03	4.11	4.12	4.00
2.11	2.06	2.03	2.04	2.10	2.13	2.11
2.49	2.50	2.58	2.56	2.67	2.66	2.73
5.58	5.39	5.24	5.19	5.06	5.06	5.01
3.75	3.77	3.87	3.84	3.96	3.97	4.07
2.65	2.66	2.68	2.69	2.75	2.76	2.82
3.60	3.60	3.69	3.70	3.84	3.85	3.89
6.69	6.60	6.67	6.84	7.10	7.19	7.14
2.56	2.54	2.46	2.52	2.53	2.58	2.62
3.15	3.12	3.14	3.19	3.32	3.35	3.39

NOTE: further details on the above calculations and the associated theory can be found in the paper “The measurement and sources of fine particle elemental carbon at several key sites in NSW over the past eight years” by Cohen et al. (2000) provided in the Appendix.

APPENDIX

15th International Clean Air Conf.
27-30 November 2000
Sydney, Australia

The Measurement and Sources of Fine Particle Elemental Carbon at Several Key Sites in NSW over the Past Eight Years.

[1]David D. Cohen, [2]Ghassan Taha, [1]Ed Stelcer, [1]David Garton, [2]Gail Box.
[1.] Physic Division, Australian Nuclear Science and Technology Organisation,
Private Mail Bag 1, Menai, NSW, 2234, Australia.
[2.] School of Physics, University of NSW, UNSW Sydney, NSW, 2052, Australia.

Summary

ANSTO has been sampling, characterising and sourcing fine particles (PM2.5) in key urban and industrial sites in NSW, twice a week, since 1991. Accelerator based ion beam analysis techniques have been used to quantify elemental components in the ambient aerosol collected for up to 25 different chemical species. One of the main constituents of atmospheric fine particles is elemental carbon (EC). In NSW urban areas this generally represents between 10 to 40% of the fine mass. It has a range of sources including biomass burning, motor vehicles, industry and fossil fuel combustion. This paper discusses the techniques, calibration and sensitivities of the transmission and the reflection measurement methods used to determine EC concentrations in ambient air. For EC generated by combustion processes an average absorption coefficient of (7±1) m^2/g was determined for particles with aerodynamic diameters below 0.5 µm. For graphite dust with particle diameters well above 1 µm a value of 1.4 m^2/g was measured.

Keywords: Elemental carbon, soot, fine particles, mass absorption coefficient, light absorption and reflection, aerosols.

1. Introduction

Atmospheric fine particle pollution has become a significant issue for discussion both nationally and internationally. In July 1997 the US EPA introduced PM2.5 national ambient air quality standards and this has helped the discussions along in many countries. The focus on fine particles has been driven by their impacts on human health, visibility, climate forcing and inter-regional transport. Australia also is developing a strong interest in fine particles in ambient urban airsheds.

Light absorption in the atmosphere is dominated by elemental carbon (EC) or soot, sometimes called black carbon. Horvath (1993, 1997b) claims that it is responsible for more than 90% of the light absorption due to atmospheric aerosols. In the atmosphere main sources of EC are anthropogenic and include biomass burning, motor vehicles and industrial sources such as coal combustion for power generation. Measurements in many urban areas in Australia (Cohen et al 1995, 1995b, 1996, 1999, Ayers et al 1998) have shown that EC is typically 10-40% of the fine mass (PM2.5) fraction. It is therefore an important parameter to measure correctly. Here we discuss and compare two simple techniques of light absorption and reflection from standard Teflon and polycarbonate filters to determine their EC content.

2. Transmission and Reflection Methods for Measurement of EC

The absorption and reflection of visible light in the atmosphere depends on the particle concentration, density, refractive index and size (Horvath 1993,1997). If we collect these particles on filter papers we can relate the mass concentration M in the atmosphere ($\mu g/m^3$) to the areal density D ($\mu g/cm^2$) on the filter in the following way,

$$D = M*V/A \qquad (1)$$

where A is the filter collection area (cm^2) and V = (60F*t/1000) is the volume of air sampled (m^3) using a pump flow rate of F (L/min) for a sampling time of t (hours). The transmission of light of a given wavelength through such a filter containing aerosol particles is given by (Edwards et al 1983),

$$I = I_0 \exp[-\varepsilon D/100] \qquad (2)$$

where I_0 is the transmission through the blank unexposed filter, I is the transmission through the exposed filter, ε is the absorption coefficient for a given wavelength (m^2/g). Note $D=\rho x$ where ρ is the density of the absorbing material (g/cm^3) and x is the material thickness (cm). For

atmospheric particles Horvath 1993 states that EC is the most highly absorbing component in the visible with very much smaller contributions from soils, sulphates and nitrates. If, to first order we assume all the absorption on our filter is due to EC then by inversion of equation (2) we get the transmission areal density of elemental carbon EC_T on the filter as,

$$EC_T\ (\mu g/cm^2) = \{100/(F\varepsilon)\}\ \ln[I_0/I] \qquad (3)$$

where ε is the mass absorption coefficient for EC (m^2/g) at a given wavelength and F is a correction factor of order 1.00 to account for the fact that sulphates, nitrates and other possible factors like shadowing and filter loading have been ignored. In all of the current work we will assume F=1.00. For reflection rather than transmission measurements on these filters the path length is twice the transmission path length and hence similar arguments lead to the reflection areal density of EC_R on the filter as,

$$EC_R\ (\mu g/cm^2) = \{100/(2F\varepsilon)\}\ \ln[R_0/R] \qquad (4)$$

where R_0 and R are the pre- and post- reflection intensity measurements at a given wavelength respectively. It is common practice to set the pre-reflection intensity R_0=100% and to rewrite equation (4) with %R=(100R/R_0). The term ln[R_0/R] then becomes {4.61-ln[%R]}.

Maenhaut 1998 defines an equivalent experimentally determined expression for EC_R using white light reflectance measurements on 47 mm diameter Nuclepore filters with ε = 5.27 m^2/g and F=1.00 and a small positive offset of 0.0523 $\mu g/cm^2$ when R_0=R.

Obviously equations (3) and (4) should produce equivalent results for EC areal density measurements on the same filters which can then be related to atmospheric mass concentration estimates via equation (1).

2.1 System Calibration

Equations (3) and (4) demonstrate that a plot of the EC areal density in $\mu g/cm^2$ on a filter versus the natural log of the ratio of pre- and post- transmission and reflection intensities should be linear with the gradient providing an estimate of the mass absorption coefficient ε appropriate to EC at the given wavelength. Fig. 1 shows such a plot for the transmission of 633nm He/Ne laser light through Teflon and polycarbonate filters artificially loaded with known amounts of smoke from a candle and an acetylene torch and spectroscopically pure graphite dust.

Clearly the plots are linear with good correlations, however the gradients are quite different for ground graphite dust and sooty carbon from the combustion of a candle or an acetylene torch. Mass absorption coefficient estimates from these gradients, assuming F=1.00, gave ε = (7.0±0.6) m^2/g for candle smoke, ε = (6.7±1) m^2/g for acetylene smoke and ε = (1.4±0.14) m^2/g for graphite dust.

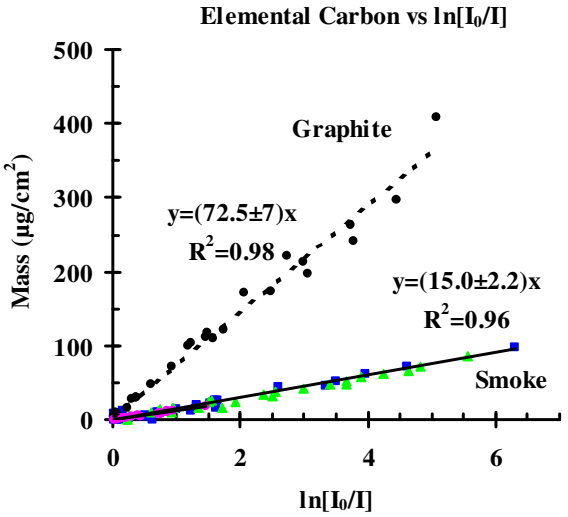

Fig.1. The transmission of 633nm He/Ne laser light through filters artificially loaded with known amounts of smoke from a candle and an acetylene torch and spectroscopically pure graphite dust.

Changes in the transmission and reflection ratios of the order of 1% or less are readily measurable with this system. A 1% change corresponds to concentrations of between 50 and 150 ng/cm^2 of EC on the filters. This is more than sensitive enough to measure typical EC values above 10 $\mu g/cm^2$.

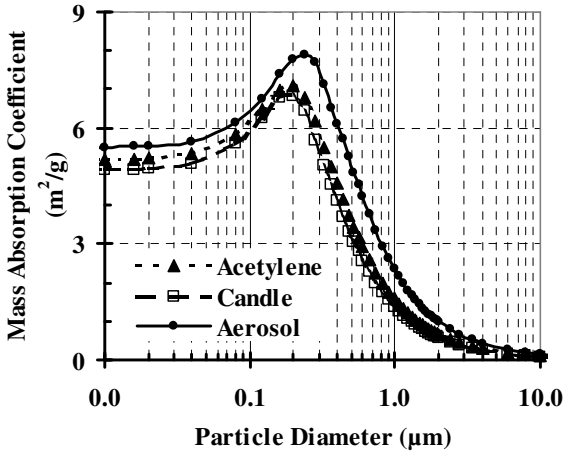

Fig.2. Calculated mass absorption coefficients for candle smoke, acetylene and atmospheric aerosols versus particle aerodynamic diameter for 633nm wavelength He/Ne laser light.

It is well known that mass absorption coefficients are dependent on particle size, density and refractive index (Horvath 1993). Fig. 2 shows calculated mass absorption coefficient variations versus particle size for typical acetylene, candle and atmospheric aerosol particles

(Horvath 1993, Fuller 1999, Taha 2000). The mass absorption coefficient falls dramatically for particle diameters above 0.5µm. The values obtained from our calibration fits of Fig. 1 are consistent with particle diameters of less than 0.5µm for the smoke generated EC and greater than 1µm for the graphite dust. Fig. 2 shows that it is only possible to use a constant value for mass absorption coefficient if the density of all particles is constant and their aerodynamic diameters are below 0.1µm. For particle diameters above 1µm the mass absorption coefficient can be an order of magnitude smaller than the fine particle value. The EC estimates, using equations (3) or (4), are inversely proportional to $\boldsymbol{\varepsilon}$ and hence strongly dependent on the value used. Generally for particles produced by combustion processes the diameters are less than 0.5µm and values of $\boldsymbol{\varepsilon}$ from 5 to 10 m^2/g are appropriate (Fuller et al 1999). Literature values of EC mass absorption coefficient range from 4 to 20 m^2/g with 10 m^2/g previously being used as the accepted value for EC from diesel smoke. However, Fuller et al 1999 suggest that this value for diesel EC maybe as much as 50% too high.

Mie theory shows there are two distinct regions of interest (Horvath 1993) define by X<1 and X>1 where $X=(\pi d/\boldsymbol{\lambda})$ is the normalised particle diameter, d is the aerodynamic particle diameter and $\boldsymbol{\lambda}$ is the wavelength of the absorbing light. In the first region, where the particle diameter is much less than the wavelength the normalised mass absorption coefficient $Q=(2d\boldsymbol{\rho\varepsilon}/3)$ is proportional to X, whereas for large particle diameters above the wavelength (X>1) Q has a constant value around 1. Hence for large particle diameters the mass absorption coefficient $\boldsymbol{\varepsilon} \propto (1/d\boldsymbol{\rho})$ or, for a fixed particle density $\boldsymbol{\rho}$, $\boldsymbol{\varepsilon}$ decreases for increasing d. This is well demonstrated in Fig. 2 for the part of the curve with particle diameters well above d=0.6µm (He/Ne laser $\boldsymbol{\lambda}$=0.633µm). For very small particle diameters $\boldsymbol{\varepsilon} \propto (\boldsymbol{\lambda}/\boldsymbol{\rho})$ and is independent of d and proportional to the absorbing wavelength for a fixed particle density. This is represented by the flat portion of the curves in Fig. 2 below d=0.1µm. For 0.1<d<0.6µm the curves show structure and the mass absorption coefficient is a function of particle diameter, absorbing wavelength and particle density.

Figs. 3 (a) and (b) show scanning electron micrographs of candle smoke and graphite dust respectively. Clearly the particle sizes in these figures are consistent with the experimental data obtained from Fig. 1. For combustion particles from smoke the majority of particles have uniform diameters between 0.1 and 0.3µm whereas the graphite dust is composed of particles all well above 1µm in diameter.

Equations (3) and (4) show that a plot of the ln[%R] for reflection versus $\ln[I_0/I]$ for transmission should be a straight line with negative slope of 2. Fig. 5 is a such a plot for both Teflon and polycarbonate Nuclepore filters. The ln[%R=100%] = 4.61 so the line should intercept the reflection axis at 4.61 and the transmission axis at 2.30 or $[I_0/I]$ = 10. The correspondence between the two methods is excellent for reflection intensities above ln[%R] > 1.

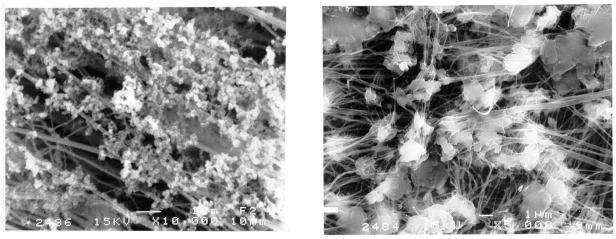

(a) (b)

Fig. 3. Scanning electron micrographs of (a) acetylene smoke on a Teflon filter, x10,000 mag and (b) graphite powder on a Teflon filter, x5,000 mag.

However the reflection intensity saturates for ln[%R]< 1 or $[100R/R_0]$ < 2.7%. This makes reflection methods for measuring EC on these two filters useless for highly loaded filters. Use of equation (4), with $\boldsymbol{\varepsilon}$ = 7 m^2/g, shows that this saturation corresponds to EC filter loadings greater than about 7 $\mu g/cm^2$.

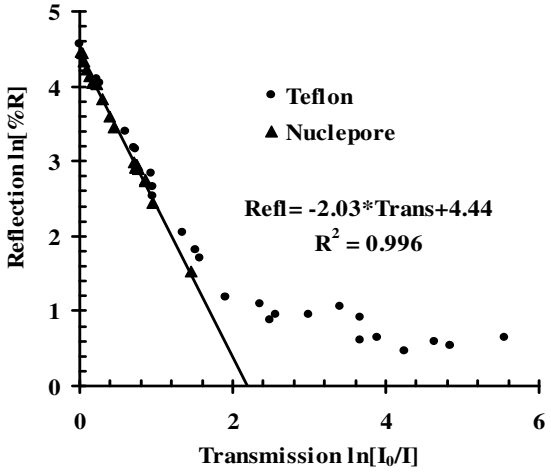

Fig. 5. Plot of log of reflection versus transmission intensities for Teflon and Nuclepore filters for 633nm He/Ne laser light.

Useful transmission measurements were obtained for $\ln[I_0/I]$ values up to 6, this corresponds to transmission intensities of less than 0.25% or using equation (3), with $\boldsymbol{\varepsilon}$ = 7 m^2/g, EC filter loading up to 86 $\mu g/cm^2$. Fig. 1 also demonstrates that the calibration, at least for fine particle EC smoke, is linear out to values of $\ln[I_0/I]$ = 6 as well. The transmission methods for EC measurement generally have a broader useful dynamic range than reflection methods.

3. Elemental Carbon Measurements

The Aerosol Sampling Program (ASP) at ANSTO has been measuring and characterising fine particles (PM2.5 and PM10) in Australia and overseas for many years now (Cohen et al 1995 1995b, 1996b, 1999). The applicability of the fast non destructive techniques of accelerator based ion beam analysis methods have been used extensively to determine over 25 different chemical species from hydrogen to lead and to define source fingerprints for fine atmospheric pollution (Cohen et al 1996, 1998, 1998b). Tens of thousands of fine particle filters have been analysed and in most cases elemental carbon estimates have been made using He/Ne laser transmission measurements and more recently white light reflection methods as described above. By measuring so many major and minor chemical species good mass closure can be obtained (Cohen 1995, 1999, Malm et al 1994). That is, the sum of all the measurement analytical species, called the reconstructed mass (RCM), is close to the total gravimetric mass measured for each filter. For the stretched Teflon filters used in the bulk of our ASP work (Cohen 1995b, 1996, 1999) the main constituents not measured are water vapour and nitrates. A comparison over many years and at a range of sites shows that RCM is about (87±21)% of the total fine particle gravimetric mass for these filters.

Fine particle sampling at sites in Wollongong, Sydney and Newcastle in NSW over the years shows that the average PM2.5 particles in these populated urban regions is composed of about 23% ammonium sulphates, 20% elemental carbon, 20% organic matter, 10% seaspray, 11% fine windblown soils and a range of trace elements 2% including metals like chrome, copper, zinc and lead (Cohen et al 1995, 1996b, 1999). Elemental carbon is therefore a major component of fine urban aerosols and as a major contributor to visibility degradation its quantification is important.

Table 1 shows the measured annual average percentage elemental carbon (PM2.5) for three sites, Warrawong in Wollongong, Mascot in Sydney and Mayfield in Newcastle over the eight year period from January 1992 to December 1999. The Wollongong and Newcastle sites are strongly influenced by industry such as steel production, but are still considered urban residential sites, whereas the Sydney site is an inner city urban site strongly influenced by motor vehicles.

The total measured mass and EC mass for each site are also given at the bottom of the Table. The average percentage EC in the total PM2.5 mass is relatively constant for all three sites over the sampling period. There are however strong seasonal variations at all sites as shown in Fig. 6 where the total mass and the EC for PM2.5 particles for the inner Sydney site at Mascot are plotted as a function of time. The EC values follow the total mass being higher in the winter months and lower in the summer months. Seasonal variations can alter both the mass and the EC by factors of 3 to 5.

	PM2.5 Annual Percentage Elemental Carbon Estimates (%)		
Year	**Warrawong Wollongong**	**Mayfield Newcastle**	**Mascot Sydney**
1992	9.7±1.3	14±2	19±2
1993	15±2	17±2	21±2
1994	(14±2)*	19±2	21±2
1995	14±2	15±2	21±2
1996	16±2	18±2	23±2
1997	13±2	16±2	23±2
1998	15±2	14±2	23±2
1999	14±2	15±2	23±2
8 yr Av.%	14±2	17±2	22±2
8yr Av. Mass	8.4±6	12±6	10±7
EC(μg/m^3)	1.2±0.8	2.0±1.3	2.3±1.7

** Only includes January and February 1994 data for the Warrawong site.*

Table 1. PM2.5 elemental carbon estimates by laser transmission, assumes ε=7m^2/g and includes an 11% correction for soil

The more than 650 filters obtained from the Mascot site over the sampling period together with the high mass closure obtained RCM=(89±9)% enables a reasonably independent estimate of the EC mass to be obtained for actual atmospheric aerosols.

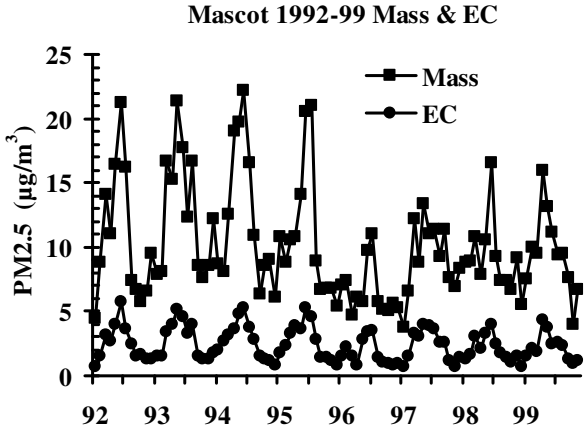

Fig. 6 PM2.5 total mass and EC for the Mascot site in Sydney from January 1992 to December 1999. EC was measured using laser transmission methods and a constant mass absorption coefficient of **ε** = 7 m^2/g as obtained from the calibration curve of Fig. 1.

If we assume that the missing gravimetric mass of 11% (i.e. 100%-89%) is composed entirely of nitrates and water vapour and add to it all measured analytes except elemental carbon, then the remaining gravimetric mass can be considered an estimate of EC in the actual aerosol. Fig. 7 is a plot of this estimated EC versus $\ln[I_0/I]$ for the Mascot site for the 8 year sampling period.

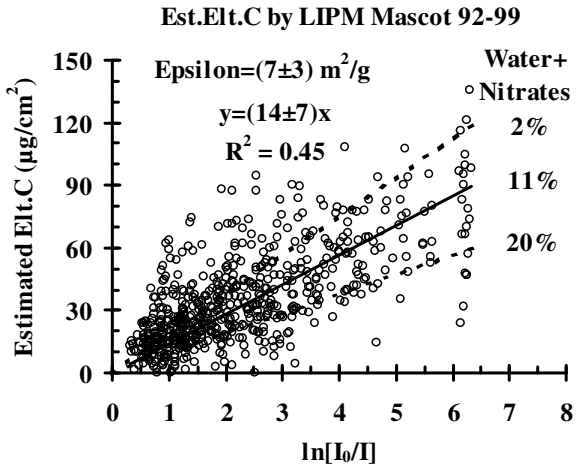

Fig. 7. A plot of this estimated EC versus $\ln[I_0/I]$ for the Mascot site for the 8 year sampling period. The solid line represents a least squares fit to the data assuming the water vapour plus nitrates were 11% of the total mass and the two dashed curves are the ±9% one standard deviations about this 8 year average.

The solid line represents a least squares fit to the data points assuming the water vapour plus nitrates were 11%, equivalent to the eight year average missing mass. The correlation coefficient for this linear fit was fair being $R^2 = 0.45$. As before, the gradient of this fit, (14±7), gave an estimate of the aerosol mass absorption coefficient at Mascot of $\varepsilon=(7\pm3)$ m^2/g. This was totally consistent with the calibration methods for smoke given in Fig. 1. The two dotted straight lines in Fig. 7 represent the one standard deviations about the solid line for the possible range of water vapour plus nitrates at the Mascot site, estimated to be (2–20%).

4. EC Size Distribution

The size distribution of EC in the Sydney region has been measured recently using a multi-stage MOUDI sampling system (Ayers et al 1998). A plot of the EC mass versus particle size is shown in Fig. 8 for a constant absorption coefficient $\boldsymbol{\varepsilon}$ over the whole particle diameter range from 0.01 to 30 µm. The discussions above have shown that $\boldsymbol{\varepsilon}$ is not constant with particle diameter but displays a variability similar to that given in Fig. 2 for a constant particle density.

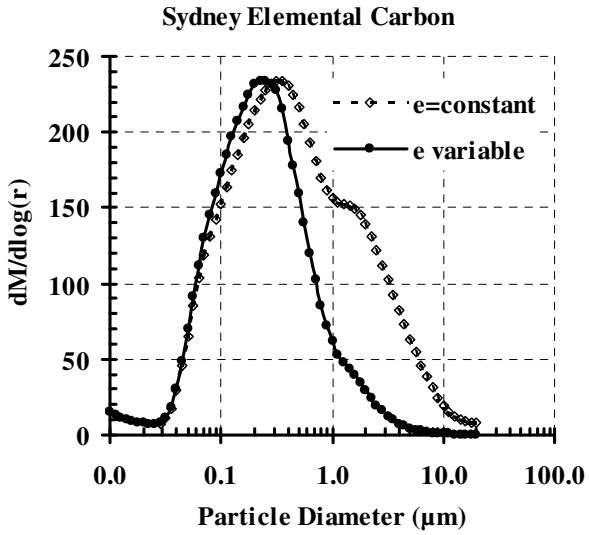

Fig. 8. A plot of the size distribution of EC in Sydney using a constant value of mass absorption coefficient (open diamonds) and a variable absorption coefficient (solid circles) similar to that shown in Fig. 2.

Below 0.1 µm the mass absorption coefficient is constant with particle diameter and the two curves of Fig. 8 differ little. However, above 0.5 µm there are strong variations with particle diameter and the curve for constant absorption coefficient over estimates the actual size distribution. In fact the full width half maximum value of the distribution is reduced from 2.92 µm (0.08 - 3.0) to 0.72 µm (0.08-0.8), with a considerably reduction over the 1 to 10 µm diameter range. A particle diameter size range that has considerable impact on the average mass of the total EC particle distribution. This is a key point for health impact studies of fine particles where differing health related issues have been associated with both PM2.5 and PM10 size particles. The peak value of the distribution is only slightly affected by the use of a variable mass absorption coefficient being between 0.2 and 0.3 µm for both situations, consistent with the combustion or smoke particle diameters shown in the scanning electron micrographs of Fig 3.

5. Conclusion

We have shown that the transmission and reflection methods for elemental carbon measurements on Teflon and polycarbonate Nuclepore filters are simple, easy to perform techniques. They are applicable to typical urban situations and are readily calibrated using filters artificially loaded with smoke from candles or acetylene flames. Great care should be taken to understand the size distribution of the elemental carbon one is measuring as the mass absorption coefficient is a strong function of particle size, density and the wavelength of the absorbing light. Transmission and reflection methods behave as expected, however transmission measurements generally

have a broader useful range of possible EC mass loadings on the filters before saturation occurs. For EC generated by smoke and for EC from the Sydney aerosol an absorption coefficient of (7±1) m^2/g was determined for particles with aerodynamic diameters below 0.5 µm. For graphite dust with particle diameters well above 1 µm a value of 1.4 m^2/g was measured.

6. Acknowledgements

We are pleased to acknowledge the support and help of the ANSTO 3MV Van de Graaff accelerator staff and the financial support of Newcastle, Botany City Councils, BHP Steel and AINSE throughout many phases of this work.

7. References

Ayers G.P., M.D.Keywood, G.L. Gras, D. D. Cohen, D. Garton and G.M. Bailey, 1998, Chemical and Physical Properties of Australian Fine Particles: A Pilot Study, Consultants Final Report to Environment Australia, April 1998.

Cohen D. D. et al, 1995, Meteorological and Chemical Interpretation of Air Pollution by Fine Aerosol Particles in the Region 200 km around Sydney. Report for Environmental Trust Grant No 1993/RD/G02, March 1995.

Cohen D. D. et al, 1995b, Energy Research and Development Corporation Study Report No ERDC 259, Vol 1-V, June 1995.

Cohen D. D., G. M. Bailey and R. Kondepudi, 1996, Elemental analysis by PIXE and other IBA techniques and their application to source fingerprinting of atmospheric fine particle pollution, Nucl. Instr. and Methods, **B109**:218-226.

Cohen D.D., 1996b, Have fine particle lead concentrations fallen in Sydney during the last 4 years? Proceeding of 13th International Clean Air and Environment Conference, Adelaide, Australia, 22-25 September 1996, pp238-244.

Cohen D. D., 1998, Characterisation of Atmospheric Fine Particle Using IBA Techniques, Nucl. Instr. and Methods, **136B**:14-22.

Cohen D. D., John L. Gras, 1998b, Characterisation and Source Fingerprinting of Fine Particle in the Jakarta Region by Ion Beam Methods, Proceedings of 14th International Clean Air and Environment Conference, Melbourne, Australia, 18-22 October 1998, p194-199.

Cohen D. D., 1999, Seasonal and regional variations in ambient fine particle concentrations and sources in New South Wales, Australia: A seven year study, Proceedings of International Congress of Biometeorology and International Conference on Urban Climatology, Sydney, Australia, p320-326, 8-12 November 1999.

Edwards J. D., Ogren J. A., Weiss R. E. and Charlson R. J., 1983, Particle air pollutants: A comparison of British "smoke" with optical absorption coefficient and elemental carbon concentration, Atmos. Environ., **17:**2337-2341.

Fuller K. A., Malm W. and Kriedenweis S. M., 1999, Effects of mixing on extinction by carbonaceous particles, J. Geophys. Res., **104:**15941-54.

Horvath H., 1993, Atmospheric light absorption – A review, Atmos. Environ., **27A:**293-317.

Horvath H., 1997, Experimental calibration for aerosol light absorption measurements using the integrating plate method – Summary of the data, Aerosol Science, **28:**1149-1161.

Horvath H., 1997b, Comparison of the light absorption coefficient and carbon measures for remote aerosols: An independent analysis of the data from the IMPROVE Network I and II., Atmos. Environ., **31:**2885-2887.

Malm W.C., J.F. Sisler, D. Huffman, R.A. Eldred, T.A. Cahill, 1994, Spatial and seasonal trends in particle concentrations and optical estimations in the US, J.Geophys. Res., **99**:1347-1370.

Maenhaut, W, Belgium, private communication, 1998.

Taha G., 2000, PhD thesis Department of Physics, UNSW, Kensington, NSW, Australia.


Australian Government
ANSTO